Check for updates

Heteroatoms in graphdiyne for catalytic and energy-related applications

Baokun Liu,†[ab] Lekai Xu,†[c] Yasong Zhao, [ID][c] Jiang Du, [ID] *[ab] Nailiang Yang [ID] *[cd] and Dan Wang [ID] *[cd]

The recently discovered carbon allotrope GDY possesses rich acetylenic bonds and unique pore structures, prompting GDY as an ideal candidate, tuning its electronic structure by introducing heteroatoms, broadening its usage in catalysis, energy storage and other fields. In this paper, we review different approaches to introduce heteroatoms into GDYs, including monodoping and co-doping, predesigned bottom-up synthesis of GDY, the anchoring of metal atoms into GDYs. Furthermore, we introduce the electronic properties' modification caused by these heteroatoms, including reduced diffusion barrier and adsorption energy, abundant active sites, high reversible capacity and cyclic stability, better rate performance and longer lifespan. Furthermore, the topological molecular structure of GDYs can be tuned through bottom-up synthesis methods with different monomers. GDY has great prospects for inclusion in energy storage devices such as sodium-ion batteries, lithium-ion batteries, lithium/magnesium sulfur batteries, and in electrocatalytic processes such as hydrogen evolution reactions, oxygen reduction reactions, and electrocatalytic nitrogen reduction reactions in important industrial reactions. At the end of this review, challenges and prospects of heteroatoms' introduction into GDY are discussed.

[a]School of Materials Science and Engineering, Henan Province Industrial Technology Research Institute of Resources and Materials, Zhengzhou University, Zhengzhou 450001, PR China. E-mail: jd@zzu.edu.cn

[b]Green Catalysis Center, College of Chemistry, Zhengzhou University, Zhengzhou 450000, People's Republic of China

[c]State Key Laboratory of Biochemical Engineering, Institute of Process Engineering, Chinese Academy of Sciences, No. 1 Beiertiao, Zhongguancun, Beijing, 100190, PR China. E-mail: nlyang@ipe.ac.cn; ldanwang@ipe.ac.cn

[d]University of Chinese Academy of Sciences, 19A Yuquan Road, 100049 Beijing, PR China

† These authors contributed equally to this work.

1. Introduction

In recent decades, with energy consumption growing and environmental problems deteriorating across the globe, carbon materials have attracted much attention worldwide and are being developed. Fullerenes, carbon nanotubes, and graphene have exhibited the potential for applications in the areas of information technology, electronics, energy storage, energy conversion and catalysis.[1–12] More recently, graphdiyne shortened as GDY, a unique carbon allotrope comprising sp and sp^2 hybridized carbon atoms, has been synthesized. Due to its

Baokun Liu received his BS degree at Northeastern University in Qinhuangdao, and then obtained his Master degree from Zhengzhou University in 2021 under the supervision of Professor Shaojun Zhang. His research interests include the synthesis and properties of graphdiyne.

Jiang Du received his BS degree at Nankai University, and then obtained his Doctor degree from University of Chinese Academy of Sciences in 2012 under the supervision of Professor Dan Wang. After graduation, he joined Professor Brian A. Korgel's group at University of Texas in Austin. His research interests include the synthesis and properties of nanowires and 2D nanomaterials. He started working at the School of Materials Science and Engineering, Zhengzhou University in 2018 as an Associate Professor.

19298 | *J. Mater. Chem. A*, 2021, **9**, 19298–19316

This journal is © The Royal Society of Chemistry 2021

Fig. 1 (a) Schematic illustration of heteroatoms in GDY. (b) The charge density plots of acetylenic bond in GDY, (D: donor, A: acceptor). (c) Electrostatic potential maps of pristine GD, Ni/GD, and Fe/GD, respectively.[73] Copyright 2018 Springer Nature Limited. (d) Structural sketches of atomic-scale nitrogen-doped GDY based on the monomer design strategy.[78] Copyright 2020 American Chemical Society.

unique electronic structure and porous structure, and more importantly, mild preparation conditions and excellent adaptability to various substrates for growth, GDY has quickly become a research hotspot.[13–24] Researchers have applied GDY in various fields, including lithium-ion batteries, catalytic converters, solar cells, and electrochemical drives, and have obtained remarkable results.[25–45]

Earlier studies show that the inherent properties of two-dimensional (2D) materials can be altered by the introduction of heteroatoms through doping. For example, the heteroatoms of N, B, P and S in graphene can influence the activity of graphene by changing bandgap, spin and charge distribution.[46–55] Compared with graphene, GDY has higher chemical activated carbon–carbon triple bonds, which may provide greater

possibilities for the introduction of heteroatoms.[56–66] While sp and sp^2 all-carbon structures endow GDY with unique chemical activity and physical stability,[67] the inherent triangular pore structure of GDY provides outstanding opportunities for anchoring heteroatoms,[68–73] which can modify the structure and properties of GDY. The charge distribution and pore structure of GDY vary with the type of doped atom and sites, making it possible to select and tune certain properties of GDY for the applications of GDY-based materials in different fields, such as catalysis and energy storage.[74–77]

Based on GDY's applications in catalysis and energy fields, this review focuses on how to introduce heteroatoms through different methods, including monodoping and co-doping by leveraging the acetylenic bond-rich structure of GDY, the

Nailiang Yang received his BS degree in Sun Yat-sen University, and then obtained his Doctor degree from the University of Chinese Academy of Sciences in 2013 under the supervision of Professor Dan Wang. His thesis has been awarded CAS Excellent Doctoral Dissertation. After graduation, he joined Professor Marie-Paule Pileni's group at Université Pierre et Marie Curie. Since 2015, he has been working in Professor Hua Zhang's group of Nanyang Technological University. His research interests include the synthesis and property research on 2D nanomaterials. Since 2018, he has started working in the Institute of Process Engineering, CAS as a full professor.

Prof. Dan Wang received his BS and MS at Jilin University (1994 and 1997) and Ph.D. at Yamanashi University (2001). He took his current position as a Principal Investigator at the Institute of Process Engineering, Chinese Academy of Sciences in 2004. His research interests are focused on the synthesis chemistry of multifunctional structure systems, including the controllable synthesis of hollow multi-shelled structures, 2D materials doping, 2D materials complexes and their applications for multi-component efficient electrodes.

This journal is © The Royal Society of Chemistry 2021

J. Mater. Chem. A, 2021, 9, 19298–19316 | 19299

bottom-up pre-designed introduction of heteroatoms during the synthesis of GDY, and anchoring of heteroatoms by taking advantage of the molecular pores of GDY (Fig. 1a). Moreover, we show the electronic structure of GDY is modified by different forms of heteroatoms: the introduction of an electron donor or acceptor in the acetylene chain would change the charge distribution. The localized electron separation will induce the attraction of electrophilic or nucleophilic substrates, which can improve the catalytic performance (Fig. 1b). While the topological pores in GDY provide defined space for anchoring heteroatoms. The introduction of metallic atoms in the triangular hole of GDY would induce a strong charge transfer between metal and GDY (Fig. 1c). Also, owing to the advantage of the bottom-up synthesis approach for GDY, the heteroatoms can be site-defined introduced. Then, the charge distribution can be significantly tuned, increasing the catalytic activity (Fig. 1d).[78] Furthermore, we also discuss the challenge and future direction in this field.

2. Heteroatoms induced tunable electronic properties: theoretical calculations

Understandings about the influence of heteroatoms on GDY at the atomic level help researchers to design catalysts and energy storage devices.[79–87] Some theoretical calculations have been carried out during the research to help researchers to interpret the effects of different heteroatoms on the structure and electronic properties of GDYs, including their band gap, hydrogen affinity and oxygen adsorption capability. For example, in 2012, Bu et al. reported stable configurations and electronic structures of GDY doped with boron and nitrogen (BN-GDY) based on first-principle calculations (Fig. 2a). The inhomogeneous π-binding in the sp–sp[2] hybrid carbon network in GDY brings its natural band gap. When BN pairs are incorporated into the sp–sp[2] hybrid network, the inhomogeneous π-binding will increase, and the band gap will change accordingly. BN combines ionic characteristics to localize electronic states and facilitate band gap modification. The band gap of the BN analogue of GDY is much wider than that of GDY. The tunability of the GDY band gap has shown its potential in the application of energy-related fields.[88]

Through (DFT) calculations, the potential of doping B and N atoms into GDY for metal-free electrocatalysts was systematically explored by Zhao et al.[89] Doped-GDYs exhibit extremely high stability due to their high cohesive energy. Meanwhile, due to their high electrical conductivity, preferred catalytic sites (sp-hybrid dopants) and low free energy for carbon dioxide activation, the catalytic performance of GDY on CO_2ER was enhanced. The catalytic performance is highly dependent on the doping site, where the hybridization of doped B and N atoms to the acetyl site of GDY makes it have a low limit potential (approximately −0.60 V) when carbon dioxide is converted to methane and (especially) ethylene. Therefore, by designing the doping sites of B and N atoms, doped GDY can be utilized as an efficient metal-free CO_2ER catalyst, which provides a new path to

Fig. 2 (a) The isosurfaces of the Kohn−Sham states of the VBM and CBM of GDY and the most stable nBN-GDYs with n = 2, 4, and 7 at the γ point. Copyright 2012 American Chemical Society. (b) Minimum energy pathways for H_2, CH_4, and CO diffusion through N-GDY. (c) Diffusion rate coefficient of H_2, CH_4 and CO permeation through the pores on N-GDY as the function of temperature (solid lines). The dashed lines are that for pristine graphdiyne and are presented for comparison.[91] Copyright 2015 The Royal Society of Chemistry.

Fig. 3 (a) Left: top view of charge density difference for B-doped GDY; right: optimized configuration for the best dioxygen adsorption on B-doped GDY. (b) Structures of up left: single Fe atom; upper right: Fe atomic pair; left lower: Fe$_3$ trimer and lower right: Fe$_4$ cluster anchored on GDY substrate. The pink and aquamarine balls represent C and Fe atoms, respectively.[92,93] Copyright 2020 Published by Elsevier B.V.

promote sustainable carbon dioxide conversion. In the same year, Gu *et al.* reported the systematic exploration of the ORR/OER electrocatalytic activity of GDY doped with N, B, P, and S through the density functional theory (DFT) calculation method.[90] The calculation results showed that the carbon atoms near the N- and S-doping sites are favored for the ORR reaction because of the modification on the charge dislocation, while carbon atoms near N- and P atoms perform as the active sites for OER owning to the high spin. Among them, the sp-N dopant is significantly important for boosting the catalytic performance in ORR, and also performs as the active site for OER. These results can guide the researchers in a direction for discovering new catalysts with high activity.

In 2015, Jiao *et al.* reported that nitrogen-doped GDY (N-GDY) can be used to purify hydrogen from CH$_4$ and CO, whereby nitrogen atoms enhance GDY's hydrogen affinity. In the process of hydrogen production by steam methane reformation, N-GDY increases the diffusion barrier of CH$_4$/CO while decreasing that of hydrogen, which enhances the hydrogen purification ability.[91] This N-GDY structure shows better H$_2$ selectivity and a higher H$_2$ diffusion rate because of a lower diffusion barrier value, as shown in Fig. 2b. To quantitatively describe the hydrogen purification performance of N-GDY, the diffusion rate coefficient across a mono-atom layered nano-mesh of N-GDY was calculated using the transition state theory, as plotted in Fig. 2c, which demonstrated that N-GDY nano-mesh has increased hydrogen purification capability.

In 2016, K. Chattopadhyay *et al.* applied dispersion force corrected DFT to study boron-doped GDY (B-GDY). Based on the comparison of their formation energies, the most favorable sites for B doping of each structure were determined. After that, the best configuration of di-oxygen (O$_2$) adsorption is calculated by analyzing the corresponding adsorption energies. It is found that during the doping process, boron atoms tend to replace carbon atoms in the benzene ring rather than the carbon atom in the acetylenic bond. Moreover, as a doping site, boron atoms, exhibit a more positive potential than carbon atoms. This can effectively promote the adsorption of O$_2$ molecules and have a beneficial effect on the electrocatalytic oxygen reduction activity of GDY (Fig. 3a).[92] This study also revealed that by configuring the doping site, the oxygen reduction activity of GDY can be adjusted.

Recently, He *et al.* studied the carbon dioxide reduction properties of iron atoms anchored GDY by DFT.[93] As shown in Fig. 3b, iron atoms are stably combined with the four carbon atoms on the two sides of the GDY's triangular hole, and the barrier of iron atoms moving to other positions is as high as 3.41 eV, which indicates that iron atoms will not aggregate when anchored to GDY. It is also found that affinity to *CO, *CHO and *OCHO can be tuned by varying the number of Fe atoms anchored in GDY, which results in catalytic efficiency and product selectivity for the CO$_2$ reduction reaction. Single iron atom sites can effectively catalyze the production of CO$_2$, providing significant theoretical support for the design of catalysts with precise atomic numbers in electrochemical

Table 1 Precursor and element, performance and parameter of doped GDYs

Year	Precursor/element	Application	Performance	Ref.
2014	NH$_3$/N	ORR in 0.1 M KOH	4.5 mA cm^{-2} at 0.05 V *vs.* RHE	29
2017	Pyridine, NH$_3$/N	ORR in 0.1 M KOH	5.1 mA cm^{-2} at 0.2 V *vs.* RHE	104
2018	Melamine/N	ORR in 0.1 M KOH	~53 mA cm^{-2} at 0.2 V *vs.* RHE	105
2016	NH$_3$/N	Reversible capacity	761 mA h g^{-1} at 500 mA g^{-1} after 400 cycles	107
2019	Pyridine/N	Cyclability	More than 350 h under a harsh working condition	108
2019	C1$_2$/C1	ECNRR	10.7 µg h^{-1} cm^{-2}	112
2019	Sublimed sulfur/S	Magnetic	Residual magnetization of more than 0.047 emu g^{-1} at room temperature	113
2019	Benzyl disulfide/S	Capacity	500 mA h g^{-1} at 500 mA g^{-1} after 200 cycles	114
2019	Phosphoric acid/P	Reversible capacity	637 mA h g^{-1} at 500 mA g^{-1} after 400 cycles	116
2019	Melamine, dibenzyl sulfide/N, S	OER	47.2 mA cm^{-2} at 1.6 V *vs.* RHE	118

This journal is © The Royal Society of Chemistry 2021

J. Mater. Chem. A, 2021, **9**, 19298–19316 | **19301**

reactions. The introduction of Fe atoms brought the highest activity and selectivity for methane generation, which is superior to most catalysts reported so far. This study shows the great potential to design the precise number of anchored atoms in GDYs as catalysts for wider applications in electrochemical reactions.

3. Heteroatom induced tunable electronic properties: an experimental approach

Heterogeneous atoms can control the local charge distribution by donating/withdrawing electrons, and electron–orbital interactions. According to different approaches in introducing heteroatoms, this part can be divided into the following types.

3.1 Introduction nonmetallic heteroatoms by post-treatment

Besides the theoretical calculations and research, as mentioned in Section 2, researchers have used doped GDYs to address key issues of reversible batteries and catalysis. For example, the

unstable electrochemical interface in the anode and cathode materials in lithium-ion batteries frequently leads to low battery efficiency. In the research of supercapacitors, the wettability of electrode surfaces is quite important. During the oxygen reduction reaction (ORR) process, slow kinetics is the main obstacle to achieving high performance.[94–103] After the introduction of heteroatoms into GDYs through doping, the electronic structure and electron mobility of GDYs can be adjusted. Molecular absorption/desorption, charge separation, and surface chemical activity can also be significantly modified as well. Herein, the precursor/element, performance, and parameters of doped-GDYs are summarized in Table 1. It can be observed that the low-cost melamine was used as the nitrogen source for doping on GDY and get the best comprehensive performance for ORR. The prepared NFLGDY-900c has a current density of about 5.3 mA cm^{-2} at 0.2 V in an alkaline environment, which is close to the commercial Pt/C.

3.1.1 Mono-doping. Nitrogen-doped GDY (N-GDY) was one of the earliest studied materials for GDY doping. Carbon atoms substituted by nitrogen atoms have been proven to be a favorable and stable configuration. Nitrogen atoms can be doped into the benzene ring and acetylene bond. The introduction of
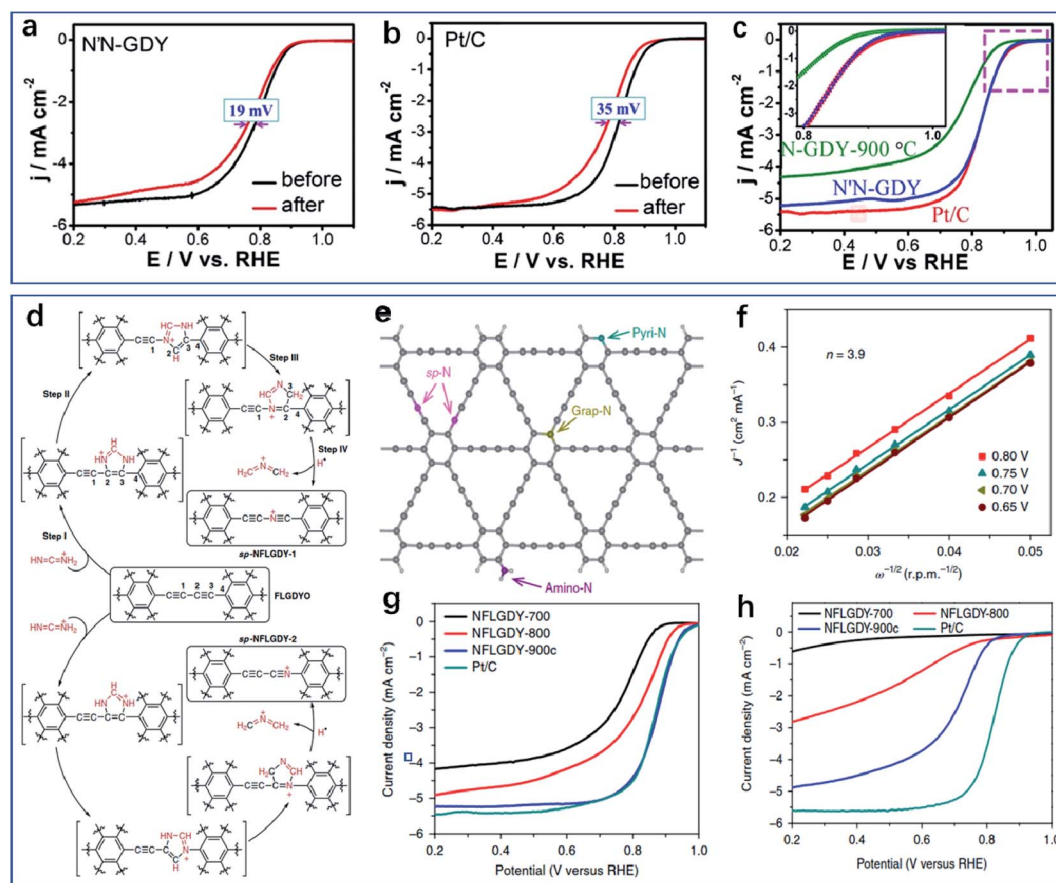

Fig. 4 Durability test of the (a) N'N-GDY and (b) commercial Pt/C for 5000 CV cycles in O$_2$-saturated 0.1 M KOH. (c) LSV curves of N-GDY-900 °C, N'N-GDY, and commercial Pt/C at 1600 rpm in O$_2$-saturated 0.1 M KOH.[104] Copyright 2017 American Chemical Society. (d) Synthesis of sp-N-doped few-layer GDY. (e) Geometries of N atoms in NFLGDY. (f) Corresponding Koutecky–Levich plots (J^{-1} *versus* $\omega^{-1/2}$). (g) Electrocatalytic ORR activity of NFLGDY and commercial Pt/C in O$_2$-saturated 0.1 M KOH. (h) Electrochemical characterization of NFLGDY and commercial Pt/C for the ORR in O$_2$-saturated 0.1 M HClO$_4$.[105] Copyright 2018 Springer Nature Limited.

19302 | *J. Mater. Chem. A*, 2021, **9**, 19298–19316

This journal is © The Royal Society of Chemistry 2021

nitrogen atoms causes a change in the local charges distribution. The carbon atoms adjacent to the doped nitrogen have higher positive charge density to counteract the strong electron affinity of nitrogen atoms, thus promoting the ORR activity.[90] The modified charge distribution will affect the ion/atoms affinity, which can be used for ion storage.

3.1.1.1 N doping. In 2014, researchers introduced nitrogen atoms into GDY (N-GDY) by annealing in an atmosphere of argon and ammonia (10% NH_3) for the first time; this experiment provided the theoretical framework for the experimental verification of heteroatom-modified GDY.[29] As a metal-free catalyst for high-performance ORR, this N-GDY exhibited better stability and cross-effect tolerance compared to commercial Pt/C catalysts. In 2017, Lv *et al.* continued to study the ORR performance of N-GDY. Pyridine was mixed with GDY to prepare N-GDY, which was then calcined in an ammonia atmosphere to obtain N′N-GDY.[104] The specific surface area of N′N-GDY was as high as 1154 m^2 g^{-1}, and the porosity is good for catalytic performance. Besides, the nitrogen content of N′N-GDY is higher than that of N-GDY, which also brings more defect sites and is thus extremely beneficial to the activity of ORR. As shown in Fig. 4a and b, after the same accelerated aging test, the half-wave potential of N′N-GDY exhibited a negative shift of 19 mV, which is far less than that of Pt/C (35 mV), thus indicating that N′N-GDY is more stable than commercial Pt/C. With an exception to this, the catalytic activity of N′N-GDY for ORR is comparable to that of commercial Pt/C catalysts (Fig. 4c).

The above research shows that N-GDY has good prospects in the field of catalysis and that it is necessary to clarify the doping configurations in the design and preparation of high-performance catalysts. As is widely known, GDY possesses rich acetylenic bonds. Therefore, it gives the possibility to design a chemical reaction for the site-defined introduction of heteroatoms. In this case, in 2018, a new form of nitrogen was introduced into GDY by precise synthesis. We introduced sp-hybridized nitrogen (sp-N) atoms into GDY quantitatively at a defined position through a pericyclic reaction and proposed the reaction mechanism (Fig. 4d).[105] First, the fragment $NHCNH_2^+$, produced by pyrolysis of melamine, was anchored to the acetylenic bond of GDY through a chemical reaction, forming a five-membered carbon–nitrogen heterocyclic ring (intermediate I, a product of step I). Then, the C1–C2 bond is broken at high temperatures to form intermediate II. In the third step, the high temperature breaks C3–C4 bonds to form intermediate III. Finally, the fragment $NHCNH^+$ is separated from the GDY system to form sp-N doped GDY (sp-NFLGDY-1) under high-temperature thermal vibration. The sp-NFLGDY-2 can also be formed through similar processes due to different adsorption sites and directions of vibration. The prepared sp-N doped GDY was used in an oxygen reduction reaction. As shown in Fig. 3e, there are various nitrogen-doping forms in NFLGDY, the catalytic performance of sp-N doped GDY was improved significantly. It can be seen from the Koutecky–Levich curve that the ORR reaction is a first-order kinetic control reaction. From the slope calculation, the electron transfer number of the reaction is 3.9. This value is close to 4 electron reactions and points to an efficient ORR reaction catalytic activity (Fig. 4f). The catalyst exhibits excellent activity under both alkaline and acidic conditions (Fig. 4g, h) and its methanol resistance and stability are better than those of commercial Pt/C. This study demonstrates that by carefully controlling the doping sites and forms introduced into GDY, the electronic properties of doped GDY can be tuned for catalysis purposes.

As a catalyst, the performance of GDY is close to that of Pt/C catalyst under alkaline conditions and slightly worse than Pt/C
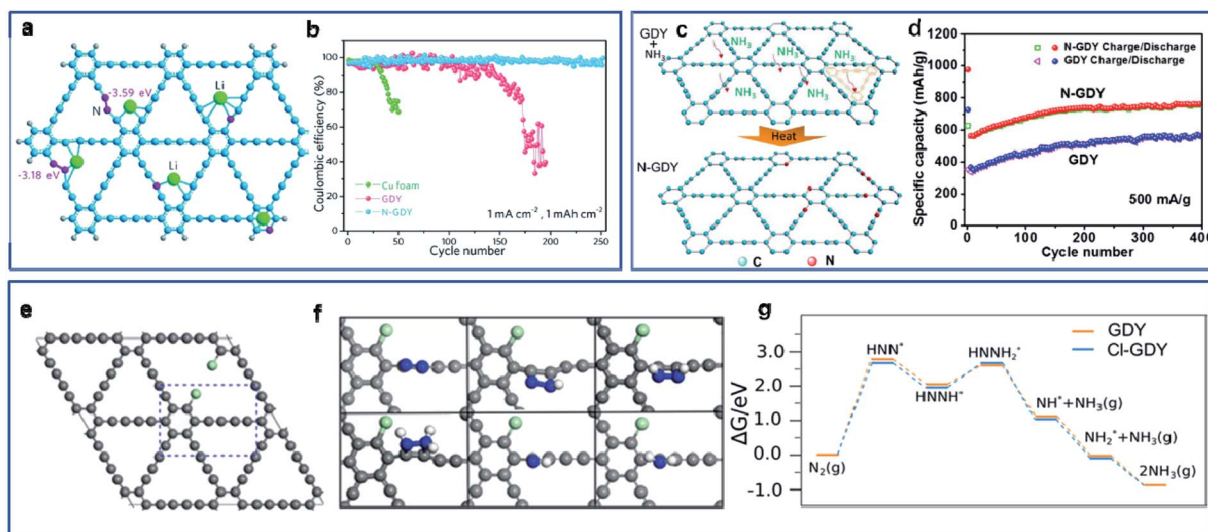

Fig. 5 (a) Optimized models of Li atom binding to N-GDY with different N-containing functional groups. (b) The Li plating/stripping efficiency of pristine Cu, GDY and N-GDY electrodes under a condition of 1 mA h cm^{-2}/1 mA cm^{-2}.[108] Copyright 2019 The Royal Society of Chemistry. (c) Schematic representation of N-doping process of GDY. (d) Cycle performance of N-GDY and GDY electrodes under 500 mA g^{-1}.[107] Copyright 2016 American Chemical Society. (e and f) Optimized structures of the Cl-GDY and intermediates. Gray, green, blue, and white spheres represent the C, Cl, N, and H atoms. (g) Free energy landscapes for N_2 reduction in GDY and Cl-GDY.[111] Copyright 2019 American Chemical Society.

This journal is © The Royal Society of Chemistry 2021

J. Mater. Chem. A, 2021, **9**, 19298–19316 | **19303**

catalyst under acidic conditions. Taking all the experimental data into consideration as well as the density functional theory calculations, it was concluded in the study that the high catalytic activity originates from the sp-N dopant. It is at this site that O_2 adsorption is facilitated and electron transfer is carried out on the catalyst surface. The addition of chemically defined sp-N atoms paves way for a new route to develop high-performance carbon-based catalysts incorporation with other non-metal elements. The activity of the GDY-based catalysts in acidic conditions is inferior to that in basic counterparts, which is because the ORR activity on N-doped carbon materials is pH-dependent. At low pH, the weak O_2 chemisorption on N-doped carbon materials makes the O–O bond dissociation impossible and the highly efficient $4e^-$ process gives way to the $2e^-$ process, leading to decreased activity.[105]

Nitrogen is introduced into GDYs not only for improving electrocatalytic performance during ORR processes, but also the performance of batteries such as zinc–air batteries and lithium batteries, including high specific capacities, outstanding rate performances, and long cycle life.[48] Lu et al. in 2021 reported the application of N-doped GDY with the stronger electropositive property as a metal-free catalyst for zinc–air batteries, which exhibits enhanced stability and polarization performance.[106] In 2015, Huang et al. used GDY powder for efficient lithium storage.[40] The rate capacity of lithium ions depends on the migration speed of electrons and lithium ions in the electrode and electrolyte. The conductivity of GDY is improved by replacing carbon atoms on the linear atomic chain and benzene ring with heteroatoms; the heteroatom defects and electrochemically-active sites of GDY are increased to achieve higher capacity.

As lithium metal is among the most promising anode candidates for high-energy-density batteries, constructing dendrite-free lithium metal anodes has become a promising strategy for developing high-performance batteries based on high lithium affinity. While most common carbon nano-materials have poor lithium affinity, the introduction of nitrogen atoms into a carbon base can improve lithium affinity.[48] Therefore, the nucleation size and position of lithium can be adjusted by introducing lithiophilic nitrogen-containing groups into GDY to significantly inhibit the growth of dendritic lithium.[107] In 2019, Jiang et al. prepared N-doped GDY nanowall-modified copper foam (N-GDY) as a highly lithiophilic substrate, and obtained a high-rate dendrite-free lithium coating with high areal capacities.[108] The model of binding lithium atoms to N-GDY is shown in Fig. 5a. Lithium metal was used as a counter electrode to assemble a semi-button cell, and the lithium affinity of N-GDY was then tested by comparing the nucleation overpotential of bare copper, GDY and N-GDY foams. It can be seen from the results of coulombic efficiency change in Fig. 5b that after 250 cycles, the coulombic efficiency of the N-GDY electrode still exceeds 98%, in contrast, the coulombic efficiency of the GDY electrode drops to 40% after 200 cycles, and the coulombic efficiency of the Cu electrode drops to 68.7% after 50 cycles. This is due to the fact that nitrogen in N-GDY has high binding energy with lithium atoms, and as a lithiophilic site, it significantly promotes uniform nucleation and deposition of lithium.

In 2016, Zhang et al. obtained N-GDY in a tube furnace filled with NH_3 at high temperatures and applied it to lithium-ion storage.[107] They gave a schematic diagram of the possible N doping sites, as shown in Fig. 5c. The local electronic structure of GDY was changed by N doping, which resulted in enhanced lithium-ion binding capacity. After 400 cycles at a current density of 500 mA g^{-1}, the reversible capacity of the N-GDY electrode was 761 mA h g^{-1}. This capacity is higher than that of GDY (559 mA h g^{-1}) (Fig. 5d). In 2018, Shen et al. used N-GDY prepared by the same method as the electrode material for lithium-ion and sodium-ion capacitors.[109] N-GDY exhibits super capacitance performance, good rate capability and excellent
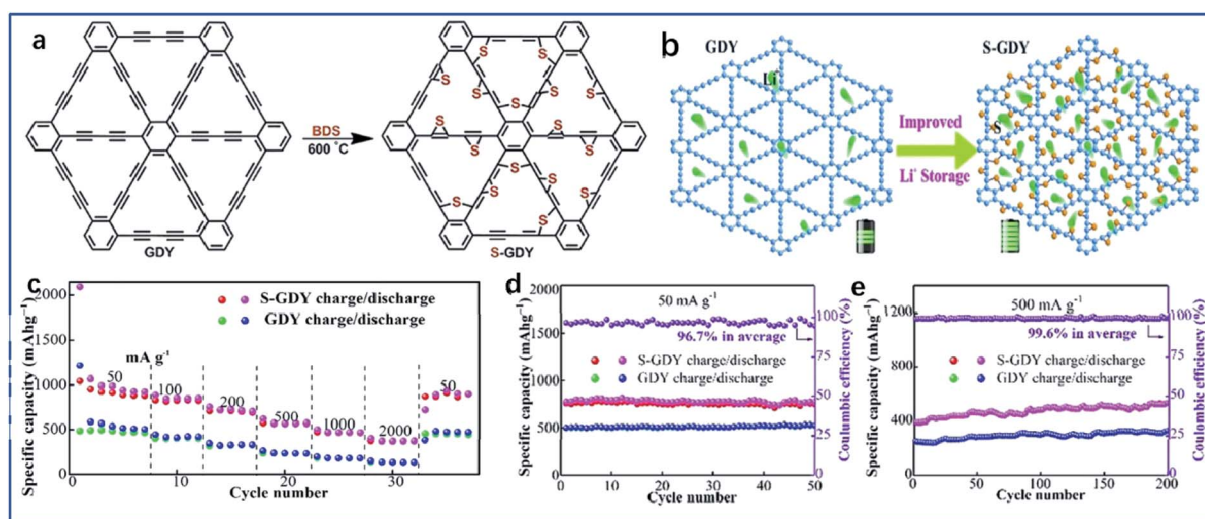

Fig. 6 (a) Schematic illustration of the preparation process of SGDY. (b) Illustration of the proposed diffusion of Li ions in GDY and S-GDY. (c) Rate performance of S-GDY- and GDY-based electrodes. (d and e) Cycle performance of S-GDY- and GDY-based electrodes under 50 and 500 mA g^{-1}.[114] Copyright 2019 Wiley-VCH.

19304 | J. Mater. Chem. A, 2021, **9**, 19298–19316

This journal is © The Royal Society of Chemistry 2021

cycle stability due to its three-dimensional porous channels, increased number of active sites, and better electrical conductivity.

3.1.1.2 Other elements doping. Besides nitrogen, other elements are also introduced into GDY in order to improve their electronic properties for certain applications. For example, chlorine is introduced into GDY to improve activity, selectivity and stability for nitrogen reduction reactions (NRRs). As is widely known, nitrogen fixation is an important step towards global sustainable development,[110] and carbon-based metal-free catalysts have been proposed to be a potential candidate for electrochemical nitrogen fixation.[111] Doping of Cl atoms is reported beneficial to the reduction of N_2, which mainly plays the following two roles: (1) redistributing electrons to adjacent carbon atoms, thus affecting the charge distribution of adjacent carbon atoms; and (2) fine-tuning the active sites of GDY, leading to the potential function with N_2 during the electrocatalytic NRR measurements. Therefore, chlorine-doped GDY is a feasible electrocatalyst for nitrogen fixation. In 2019, Duan's team prepared chlorine-doped ultra-thin GDY (Cl-GDY) through the Cl_2 corrosion method.[112] It was suggested that chlorine not only serves as a doping element but also etches GDY into thin slices in the reaction process. The carbon–carbon triple bond is the active site of N_2 activation and reduction, and the acetylenic bond will break when Cl_2 is treated at high temperature, thus forming Cl-GDY (Fig. 5e and f). The free energy during the N_2 reduction process is shown in Fig. 5g and is derived through the DFT calculation. It can be seen that the limiting step is the first proton-coupling electron transfer to N_2. After Cl doping, the

formation energy of HNN* decreases by 0.11 eV, which indicates that Cl doping is beneficial for the reduction of N_2.

Sulphur atoms are also introduced into the carbon skeleton as it is beneficial for effective interaction with electrolyte ions and improves lithium affinity and conductivity. In 2019, Zhang *et al.* prepared sulfide GDY (SGDY) and studied room temperature ferromagnetism of SGDY semiconductors.[113] In the same year, Yang *et al.* used benzyl disulfide (BDS) as a sulfur source to synthesize S-GDY (Fig. 6a).[114] The sample they prepared had only one type of S atom in the form of a C–S–C bond, which could provide a more heteroatom defects and active sites. This S-GDY is used in lithium-ion batteries to improve their storage capacity (Fig. 6b). When the current density is between 50 and 2000 mA g^{-1}, S-GDY presents better reversible capacity and rate capability than non-doped GDY (Fig. 6c). At a current density of 50 mA g^{-1}, the capacity of the S-GDY electrode is about 810 mA h g^{-1} after 50 cycles. At a current density of 500 mA g^{-1}, the capacity of the S-GDY electrode also reaches 500 mA h g^{-1} after 200 cycles (Fig. 6d and e). Through chemical modification, heteroatoms are covalently bonded to carbon atoms without introducing other impurities. This structure also provides inspiration for the design of high-performance lithium/ magnesium–sulfur batteries, wherein S-doped GDY can be applied as a compatible cathode.

The introduction of phosphorus in the carbon material is beneficial to form a thin and dense solid electrolyte interface layer on the carbon surface, thus improving the electrochemical properties.[115] Shen *et al.* prepared phosphorus-doped porous GDY (P-GDY) by calcination and applied it to lithium-ion
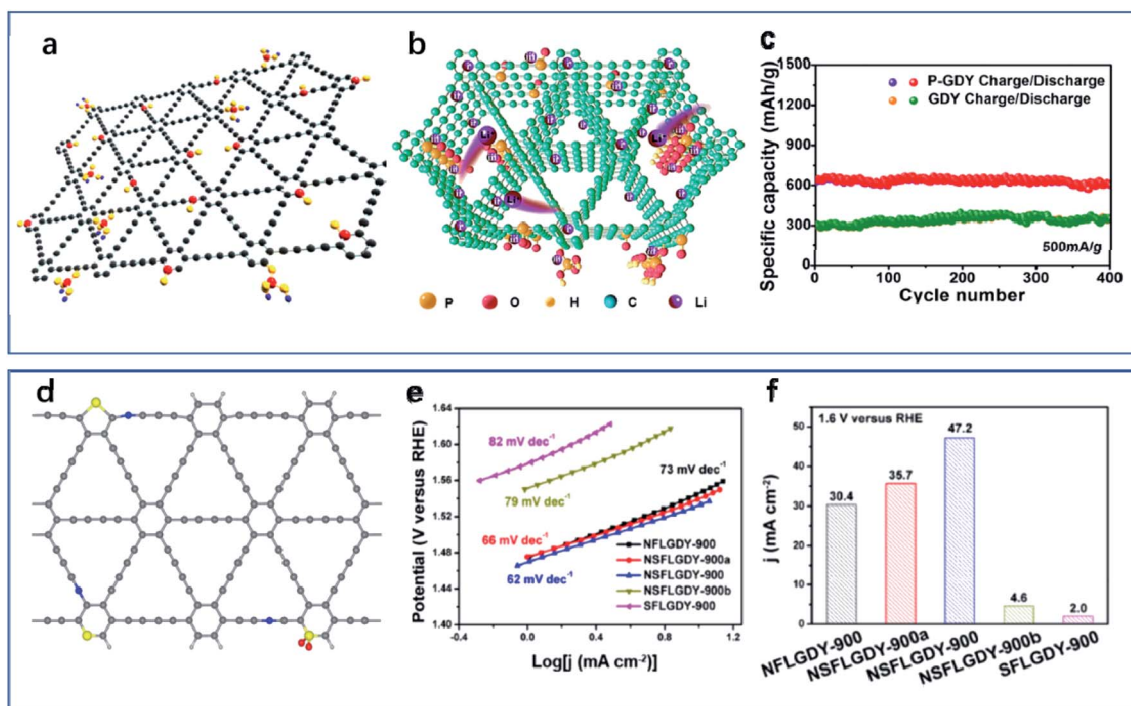

Fig. 7 (a) Schematic illustration of P doped GDY structure. (b) The mechanism of Li storage and Li-ion diffusion. (c) Cycle performance of P-GDY and GDY electrodes under 500 mA g^{-1}.[116] Copyright 2019 IOP publishing. (d) Geometries of stereo-defined sp-N, S codoped GDY. (e) Tafel plots of catalysts. (f) Current density of catalysts at 1.6 V (*versus* RHE).[118] Copyright 2019 American Chemical Society.

This journal is © The Royal Society of Chemistry 2021

J. Mater. Chem. A, 2021, **9**, 19298–19316 | **19305**

storage.[116] Due to the low electronegativity of P atoms, its doping in GDY will cause the charge to be biased towards C atoms. DFT calculations show that P-doping has a more stable configuration at the benzene ring (Fig. 7a). P-doping in the lattice of the carbon material will cause the carbon structure to become highly distorted and it will form many open edge sites and wrinkles. This will lead to a further increase in the porous structure of P-GDY, which in turn facilitates the storage and transfer of alkali metal atoms. As marked in Fig. 7b, Li atoms can be adsorbed above the center of the benzene ring and the butadiyne sites of P-GDY. In addition, Li atoms may be adsorbed near the phosphorus oxygen groups. The doping of P is beneficial to stabilize the embedded Li atoms in P-GDY, thus improving the capacity of the battery. Under a current density of 500 mA g^{-1}, the capacity of the P-GDY electrode was 637 mA h g^{-1} after 400 cycles (Fig. 7c). Therefore, doping using phosphorus is also an effective method for improving the electrochemical performance of carbon-based materials.
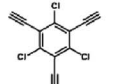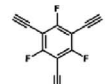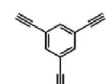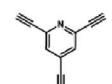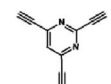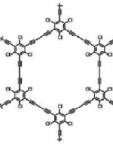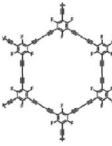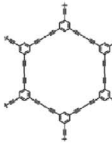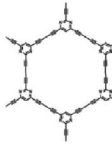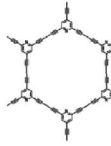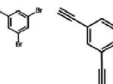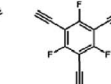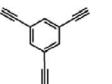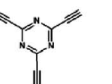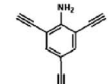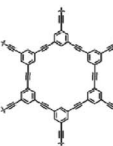
3.1.2 Co-doping. During the development of metal-free catalysts, dual-element-doped carbon nanomaterials are demonstrated to be efficient in catalyzing two key chemical reactions: ORR and oxygen evolution reaction (OER) in regenerative fuel cells and metal–air batteries after N–S, N–Cl, N–B, and N–P co-doping are carried out for carbon nanomaterials. Different from monodoping, two or more heterogeneous elements introduced into carbon materials will result in a synergic effect on improving the catalytic performance. A synergistic effect will occur within a certain distance between the codopants. For example, after N and S are introduced into a carbon nanomaterial, a strong synergistic effect is observed when the distance between N and S is generally not more than 7.5 Å.[117] Moreover, an activity descriptor can be established to correlate doping structures to catalytic activities, which can be used for the rational design of new bifunctional catalysts.[114]

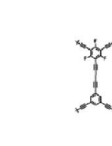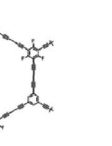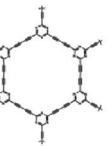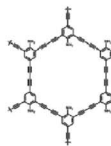As a continuation of the aforementioned work carried out by our research team, we further introduced sulfur atoms and sp-N atoms into GDY to improve catalytic performance for OER. We then analyzed the relationship between the stereoscopic distance of S and N atoms and their synergistic effects[118] (Fig. 7d). The introduction of sp-N can significantly reduce the overpotential of the catalyst, while the introduction of S atoms increases the current density of OER, bringing remarkable catalytic activity and faster kinetics. The faster kinetics are reflected in the smaller Tafel slope of NSFLGDY-900 (with relatively high concentrations of sp-N and S), as shown in Fig. 6e. The synergistic effect of this dual doping and stereodefined position resulted in the current density of GDY being higher than that of GDY doped with a single N or S element (Fig. 7f) and was even better than commercial ruthenium oxide catalysts.

3.2 Introduction nonmetallic heteroatoms by a bottom-up method

As discussed above, heteroatom-doped GDY exhibits excellent catalytic and energy storage performance owing to their modified electronic properties. However, the introduction method still meets the challenge in the introduced site control. Therefore, researchers have started to predesign how to introduce heteroatoms into GDY to obtain specific electronic properties for different applications. For example, by taking advantage of the ease of bottom-up chemical synthesis of GDY, it is possible to introduce various heteroatoms to GDY, obtaining different properties. By selecting suitable monomers to conduct the coupling reaction, the pores of the obtained GDY can be adjusted, giving great prospects for applications in the field of energy storage. The monomer structures used for predesigned GDY are summarized in Table 2.[120,121,124,128–130,132,133]

Table 2 Macroporous structures of GDY prepared by different monomers

Monomer					
Structure					
Ref.	[120]	[121]	[124]	[129]	[129]
Monomer					
Structure					
Ref.	[128]	[130]	[132]	[133]	

Previous research showed that when GDY is used in ion storage, the AB stacking mode of GDY will cause delayed ion diffusion, however, its larger pore diameter is conducive to the diffusion of ions in the material.[119] Therefore, it is possible to increase the pore size of GDY by introducing heteroatoms to allow smoother ion diffusion. At the same time, the introduction of heteroatoms enhances GDY's ion affinity, which is beneficial for increasing battery capacity. The pore size of GDY is regulated by controlling the monomer structure. Moreover, lithium storage can be improved by regulating the number and distribution of introduced heteroatoms.[120]

As halogen functionalization of carbon materials paves the way to optimize the conductivity, band-gap, and morphology properties of carbon materials due to the different electronegativities and atomic size of the halogen atoms, it has drawn much attention recently.[120] Next, we will review the pore structure and electronic properties of various GDY predesigned by different monomers.

The introduced chlorine in the carbon structure enables precise tuning of the molecule pore size and conductivity of the carbon material.[120] In 2017, Wang *et al.* utilized a coupling reaction to make 1,3,5-(trimethylsilyl)ethynyl-2,4,6-trichlorobenzene as a monomer to prepare chlorine-substituted GDY and applied it to lithium-ion storage.[120] As shown in Fig. 8a, Cl-GDY has a large hexagonal hole with an effective hole diameter of 1.6 nm. It provides a channel for the vertical diffusion of lithium ions. At the same time, the possible intercalation of lithium on Cl-GDY was studied by DFT calculation. Fig. 8b shows the four configurations when only one lithium atom is intercalated. It can be seen from the binding energy that in the Cl-GDY system, the Li complex on the acetylenic bond is more stable than that on the benzene ring, and when additional Li is provided (configuration B1), the binding energy is −1.39 eV, which indicates the stabilizing effect of Cl on Li atoms in an acetylenic bond. It can also be observed that Cl is evenly distributed across the entire GDY planar 2D network, generating more storage sites for Li ions. This has also been verified by the experimental results. Moreover, the Cl-GDY film exhibits excellent capacity retention. When the current density is 2 A g^{-1}, the reversible capacity reaches 500 mA h g^{-1} after 100 cycles (Fig. 8c), making Cl-GDY a remarkable candidate for Li-ion batteries.[120]

Compared to chlorine, fluorine has an extremely high electronegativity, which can provide maximum charge polarization
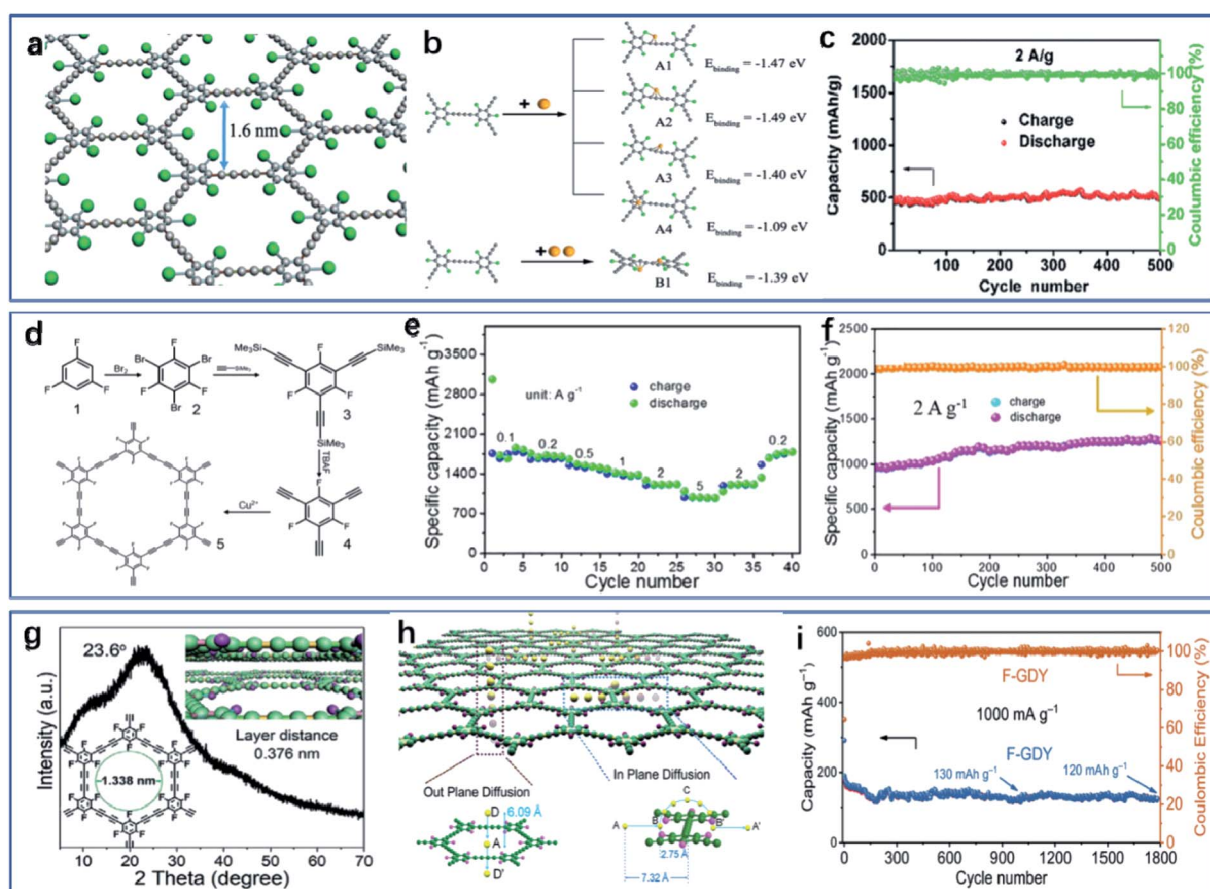
Fig. 8 (a) The structure of the Cl-GDY. (b) The geometries and formation energies ($E_{binding}$) of four optimized Li + $C_{28}Cl_6$ (A1–A4) complex and one optimized 2Li + $C_{28}Cl_6$ (B1). (c) The cycle performance of the flexible electrode at 2 A g^{-1}.[120] Copyright 2017 Wiley-VCH. (d) The synthesis route of F-GDY. (e) Cycling stability at a current density of 0.1 A g^{-1}. (f) Cycling stability at a current density of 2 A g^{-1}. Copyright 2019 Wiley-VCH. (g) XRD pattern and the schematic structure of F-GDY. (h) Diffusion barrier for the movement of K atom in F-GDY layers. (i) The cycle performance of F-GDY at current densities of 1000 mA g^{-1}.[121,123] Copyright 2020 Wiley-VCH.

This journal is © The Royal Society of Chemistry 2021

J. Mater. Chem. A, 2021, **9**, 19298–19316 | **19307**

to enhance energy-related electrochemical activity and stability. At the same time, fluorination can improve the mechanical properties and wettability of carbon-based materials. Therefore, doping of fluorine into GDY is expected to improve its electrochemical performance as a lithium storage material. In 2019, Shen *et al.* used a bottom-up method to prepare fluorine-substituted GDY (F-GDY) using a solvothermal method.[121] The synthesis route of F-GDY is shown in Fig. 8d. The pore size distribution of F-GDY is mainly 1.33 nm. Coulomb attraction between carbon atoms and fluorine atoms leads to C–F semi-ionic bonds, which enhances the conductivity. The existence of C–F bonds can effectively enhance the mechanical properties of the SEI film formed on the interface between the electrolyte and electrode. When F-GDY is used as positive electrode material in lithium-ion storage devices, the decomposition of the electrolyte and the increment in the thickness of the solid electrolyte interphase (SEI) membrane is greatly suppressed, simultaneously increasing active sites and improving the rate capability and cycle stability of the device. The rate performance of F-GDY was found to exhibit superior rate capability and stability (Fig. 8e), whereby as the current density returns to 0.2 A g^{-1}, the specific capacity returns to its initial value. Similar to what has been observed with Cl-GDY, the substitution of fluorine increases the pore size on the 2D plane of GDY and improves the storage capacity of lithium ions (Fig. 8f).

Similarly, in 2019, Kang *et al.* prepared F-GDY by mixing and annealing XeF_2 with GDY.[122] Fluorine was doped in a benzene ring and acetylenic bond. In addition to introducing a more atomic defects and electrochemical active sites, the elastic modulus of F-GDY is doubled in contrast to the pristine GDY (7.92 for F-GDY, and 4.12 for GDY). This remarkable mechanical change is helpful for improving the reversible capacity and electrochemical stability of F-GDY during cycling. With F-DGY as the cathode material of lithium-ion battery, the capacity reaches about 1080 mA h g^{-1} at a current density of 500 mA g^{-1} after 600 cycles.[122]

The introduction of F into GDY helps to improve the electronic properties for applications in not only lithium-ion batteries but also potassium ion batteries.[123] Compared to Li ions, K ions have a larger ionic radius, and the stable storage and diffusion of K ions require the design of electrode materials with regular channels, convenient diffusion channels, a large volume of expansion space, and good interface compatibility. Introducing F atoms into GDY may meet these requirements. In 2021, He *et al.* prepared F-GDY with a large aperture of 1.338 nm and an interlayer spacing of 0.376 nm (Fig. 8g).[123] The DFT calculations show that energy barriers of K atom diffusion in the F-GDY layer are 0.22 eV (in-plane) and 0.07 eV (out-of-plane), which are lower than those for Li atom diffusion in many carbon materials (Fig. 8h). F-GDY has good electrochemical performance due to its aligned ion diffusion channels and good interface compatibility. Lastly, the capacity of 120 mA h g^{-1} after 1800 cycles at 1000 mA g^{-1} was achieved (Fig. 8i). These findings provide new insight into the design of an electrode for K ion batteries.[123]

Besides the introduction of halogen elements into GDY as discussed above, the introduction of hydrogen into GDY (HsGDY) has also been experimented with to modify electrode surfaces for Zn batteries.[124,125] Introducing hydrogen atoms into benzene rings has the following advantages. Firstly, the formation of a perfect π conjugated system generates the semiconductor nature of HsGDY. Secondly, HsGDY has a large six-membered ring with a theoretical diameter of 1.63 nm, constituting the tunnels for Zn^{2+} transport together with the microgaps between adjacent HsGDY microdomains. Thirdly, the strong covalent bonds in the HsGDY network and the formation of an integrated film give stability to the HsGDY to eliminate the crushing of the slurry coating during the long-
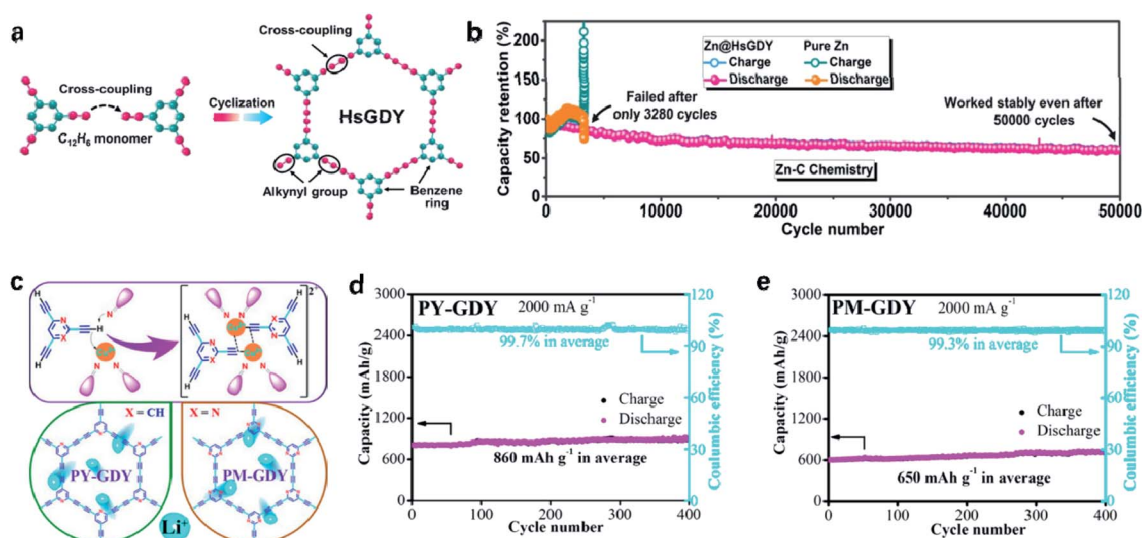
Fig. 9 (a) Schematic illustration of the synthesis of HsGDY. (b) Discharge and charge capacity retentions of Zn@HsGDY//C and Zn//C cells.[124] Copyright 2020 Wiley-VCH. (c) Possible reaction pathways in the synthesis process of PY-GDY and PM-GDY. (d and e) Cycle performance of PY-GDY and PM-GDY-based electrodes at the current density of 2000 mA g^{-1}.[129] Copyright 2018 American Chemical Society.

19308 | *J. Mater. Chem. A*, 2021, **9**, 19298–19316

This journal is © The Royal Society of Chemistry 2021

term operation.[124] Therefore, Yang et al. chemically coupled HsGDY and Zn electrodes (denoted as Zn@HsGDY) in 2020 (Fig. 9a),[124] the purpose of which was to mediate the redistribution of the Zn^{2+} concentration field and fundamentally eliminate Zn dendrites. Under a symmetrical structure, the life of the Zn@HsGDY electrode is >2400 h, and it can remain stable even at a commercial-grade cathode-loading mass of up to 22.95 mg cm^{-2} (Fig. 9b). It is utilized to solve the dendrite issue faced by various metal batteries (such as those containing zinc, lithium, sodium, or aluminum).

Research is carried out on the application of HsGDY not only in Zn batteries but also in Li-ion, Na-ion, Li–S batteries and reversible batteries. In 2017, He et al. used HsGDY in lithium-ion and sodium-ion batteries. The results presented excellent cycle performance, high reversible capacity, and superior rate performance.[126] In 2021, Kong et al. studied the performance of HsGDY in Li–S batteries. The strong physical adsorption and chemical anchoring of HsGDY material to LiPSs promoted the conversion reaction of lithium polysulfides (LiPSs) and alleviated the shuttle problem of LiPSs. As the carbon interlayer of Li–S battery, this material shows excellent stability.[127] In 2021, Ren et al. prepared HsGDY with large micropores and micropore density, which provides sites and channels for ion storage and transmission.[128]

Moreover, the qualitative and quantitative heteroatom introduction can also be achieved using the specific monomer by controlling the element type and content in the precursor molecule structure. For example, in 2018, Huang's research group used two different monomers to prepare pyrimidine-GDY (PM-GDY) and pyridine-GDY (PY-GDY) to introduce N into GDY, and used them as anode materials for lithium-ion batteries.[129] As shown in Fig. 9c, both PY-GDY and PM-GDY prepared with 2,4,6-tris(trimethylsilyl)ethynylpyridine and 2,4,6-tris(-trimethylsilyl)ethynylpyrimidine, respectively, possess a large hexagonal pore structure, which has advantages for lithium-ion storage. The cycle performance of the electrodes was verified through experiments (Fig. 9d and e), where PY-GDY-based electrodes exhibited a reversible capacity about 860 mA h g^{-1} for 400 cycles at 2000 mA g^{-1}, and PM-GDY-based electrodes obtained 650 mA h g^{-1} for 400 cycles, with both electrode materials presenting high coulombic efficiency. This excellent performance originated from the high conjugation of the two materials, the large number of doped nitrogen atoms, and a uniform hexagonal pore structure.
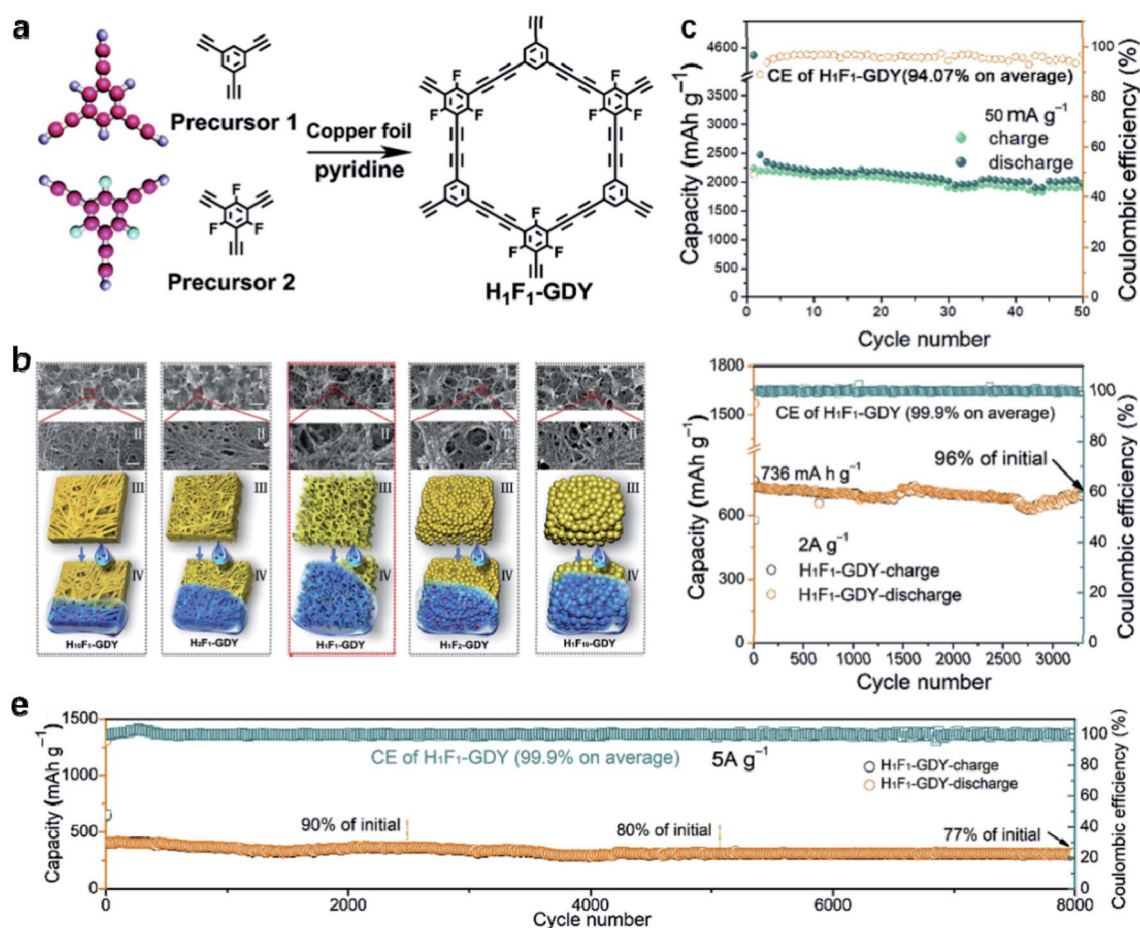

Fig. 10 (a) Schematic diagram for the preparation of H_1F_1-GDY and the ball–and–stick model of two precursors. (b) Schematic diagram of the regular morphology changes of H_xF_y-GDY. (c) The cycle performance at 50 mA g^{-1}. (d) The stability of H_1F_1-GDY at 2 A g^{-1}. (e) The cycle performance of H_1F_1-GDY at 5 A g^{-1}.[130] Copyright 2020 Published by Elsevier B.V.

Besides, various attempts have been made by researchers to co-dop different elements into carbon base to satisfy a specific demand. Structural design, positioning doping, or multiple doping are common methods used in improving the electrochemical performance of carbon materials in lithium-ion batteries. Inspired by dual doping, dual-heteroatom-based predesign is also an effective way to ameliorate the GDY structure. This method can not only control the substitution sites of heteroatoms but also take advantage of the synergic effect between different heteroatoms.

As carbon materials doped with H have a high theoretical specific capacity, and fluorocarbons demonstrate high chemical and thermal stability, weak intermolecular action and small surface energy due to the strongest electronegativity of fluorine.[130] In a subsequent study in 2020, Lu *et al.* prepared H and F co-doped GDY by mixing and coupling H-substituted and F-substituted monomers.[130] As shown in Fig. 10a, when the molar ratio of the two precursors is 1 : 1, the cross-coupling reaction to prepare H_1F_1-GDY is performed on copper foil. The main pore size of H_1F_1-GDY is 0.74 nm. The presence of H element can effectively cause lithium ions to combine and increase the lithium storage capacity. The existence of F element improves the wettability of organic electrolytes, accelerates ion transfer, and improving battery stability. The authors also investigated the influence of the surface structure of materials with different H and F ratios on interfacial wettability and diffusivity (Fig. 10b). The synergistic effect of the positioning co-doping at the ratio of H/F 1 : 1 is a significant improvement in comparison with other ratios. The large specific surface area and high porosity of the H_1F_1-GDY structure provide abundant ion transport channels and active sites for lithium storage. Moreover, the unique porous network also improves electrolyte permeability. A rough surface has been found to be beneficial in reducing surface tension and enhancing the diffusion of electrolyte, therefore improving its stability as LIBs electrode material. A series of experiments demonstrated that at a current density of 50 mA g^{-1}, the capacity was maintained at 2050 mA h g^{-1} even after 50 cycles (Fig. 10c). At a current density of 2 A g^{-1}, the capacity remained close to 96% after 3200 cycles (Fig. 10d), while in the case of 5 A g^{-1}, the capacity declined only by 23% after 8000 cycles (Fig. 10e).

In addition, introducing dual heteroatoms can also be achieved by using two monomers with different substitution positions. For example, one monomer has heteroatoms substituted for hydrogen atoms on the benzene ring, and another monomer has heteroatoms substituted for carbon atoms on the benzene ring. In 2020, Gao *et al.* used a combination of two monomers with different substitution positions to prepare doped-GDY with a precise and controllable N/C atomic ratio.[131] The presence of H atoms increases the pore size of GDY, while N in the material exists in the form of pyridine-N. Pyridine-N is instrumental in the storage of lithium and sodium ions, and so the material achieves significant lithium and sodium ion storage capacity. This design can further explain the role that heteroatoms played in lithium/sodium ion storage. In addition, in 2018, Li's team successfully introduced triazine-like N cluster into GDY through monomer design, which has high energy density when used as electrode material of capacitor.[132] In order to prepare 2D carbon nanofilms with molecular selectivity and good compatibility with Nafion at any thickness, amino groups have also been introduced into graphdiyne, and this aminated GDY(NH_2-GDY) has been successfully applied in fuel cells.[133]

3.3 Introduction of metallic atoms by anchoring

Single-atom catalysts possess high activity and selectivity, so they have been widely used in many industries as heterogeneous catalysts. Zhang reported pioneering work on Pt_1/FeO$_x$ single-atom catalysts,[134] SACs have been extensively studied in computational simulation and practical applications. Atomic catalysts (ACs) are expected to provide a key method to utilize each metal atom. However, with the decrease of metal particle size and the increase of surface free energy, metal atoms tend to form clusters. Consequently, it is necessary to prevent this aggregation while also maintaining the excellent catalytic performance of single-atom catalysts. It is also important to provide solid support to stabilize single atoms.[135] The unique alkyne-rich structure endows GDY with many attractive properties, and the uniformly distributed pores make GDY an ideal support for SACs with large binding energies to metal atoms. Herein, the anchored element, applications, and performance are summarized in Table 3 below. Both Mo- and Pd-GDY possess good catalytic performance. For Pd-combined GDY, the average yield of NH_3 can reach 4.45 ± 0.30 mg$_{NH3}$ mg$_{Pd}^{-1}$

Table 3 Element, application and performance of anchored GDY

Year	Element	Application	Performance	Ref.
2019	Mo	ECNRR	145.4 µg$_{NH_3}$ g$_{Mo}^{-1}$ h^{-1}	137
2020	Pd	ECNRR	4.45 ± 0.30 mg$_{NH_3}$ mg$_{pd}^{-1}$ h^{-1}	138
2021	Pd	ECNRR	115.93 mg$_{NH_3}$ g$_{pd}^{-1}$ h^{-1}	139
2019	Pd	4-NP reduction reaction	Rate constant k reaches 0.953 min^{-1}	140
2019	Co–N	ORR	4.01 mA cm^{-2} at 0.2 V *vs.* RHE	141
2019	Fe–N	ORR	5.4 mA cm^{-2} at 0.2 V *vs.* RHE	142
2020	Pd	Hydrogenation properties	TOF of 6290 h^{-1}, a selectivity of 99.3% at 100% conversion	143
2020	Ru	HER	Deliver 10 mA cm^{-2} at a low overpotential of 44 mV	144
2020	Fe	CO$_2$ER	Calculation	145
2021	Ni/Cu	CO oxidation	Calculation	146

19310 | *J. Mater. Chem. A*, 2021, **9**, 19298–19316

This journal is © The Royal Society of Chemistry 2021

h^{-1} and 115.93 mg g^{-1} h^{-1}, respectively. For Mo^0/GDY, the yield of NH_3 is 145.4 μg mg_{cat}^{-1} h^{-1}. For the preparation of electrocatalytic oxygen reduction catalysts, Fe- and N-GDY possess good oxygen reduction performance. The prepared 1.5% Fe–N-GDY has a current density 5.4 mA cm^{-2} at 0.2 V in an alkaline environment.

The uniform pore structure and large binding energy to metal atoms proffer GDY as an ideal carrier for single-atom catalysts. This has been verified by He *et al.* on the transition metal anchor sites on GDY.[136] Fig. 11a indicates that three possible adsorption sites for transition metal atoms (TM): (1) the TM atom is anchored in the center of a large triangle ring (S_1); (2) the TM atom is connected to four carbon atoms at the corners of the acetylenic ring (S_2); (3) the TM atom is located in the benzene ring (S_3). For the S_1 site, TM is easily transferred to S_2, which is unstable. For the S_3 site, the van der Waals force between TM and the C atom cannot be stably anchored. Therefore, the most stable and active position is the S_2 site. The authors also calculated the binding energy between TM atoms (from Sc to Zn and Pt) and a single GDY layer, as shown in Fig. 11b. With the exception of Zn atoms, the binding energies between the studied TM atoms and GDY are all negative, which indicates that there is strong chemical adsorption between TM atoms and GDY and that the diffusion of anchored TM atoms from their stable position to another position is very difficult.[136]

As the synthesis of NH_3 with high selectivity and yield under normal temperature and pressure still face many challenges, atomic catalysts have many advantages and are expected to become transformative next-generation catalysts. Hui *et al.* studied the effects of electrocatalytic nitrogen reduction reactions (ECNRR) and hydrogen evolution reaction (HER) of zero-

valent molybdenum atoms (Mo^0/GDY) anchored on GDY.[137] The experiment adopted anchor sites based on the C–C triple bond interaction because this requires lower energy costs than other locations. DFT calculations show that GDY anchors Mo^0 atoms through strong p–d coupling (Fig. 11c). In the ECNRR process, the rapid and reversible charge transfer between the Mo site and the specific C site inhibit the forward HER process. In 0.1 M Na_2SO_4, the yield of NH_3 can reach 145.4 μg $h^{-1}mg_{cat.}^{-1}$ and Faraday efficiency (FE) > 21% (Fig. 11d and e). At the same time, Mo^0/GDY can also drive efficient HER in non-N_2-saturated solutions. In 0.5 M H_2SO_4, Mo^0/GDY showed higher HER activity than commercial 20 wt% Pt/C (Fig. 11f and g).[137]

In 2020, Yu *et al.* anchored zero-valent palladium (Pd) metal atoms on GDY (Fig. 12a) with a two-way cross linear response method[138] and applied the obtained Pd-GDY catalyst in electrocatalytic ammonia synthesis, obtaining a high selectivity and ammonia yield. GDY has abundant chemical bonds, highly conjugated π electron delocalization and pore structure. With these characteristics, the researchers proposed a "metal ion anchoring-electron transfer-self-reduction" zero-valent metal stabilization process. Thereby realizing the incomplete charge transfer between the metal atom and GDY, the number of catalytic active sites is maximized, and the active components are highly dispersed, resulting in the best catalytic effect. The origin of the excellent catalytic activity of the sample was further studied through calculation (Fig. 12b). The strong orbital interaction between the Pd atom and the adjacent C site results in the strong negative reduction characteristics of ECNRR. The downward shift of the electronic structure of the s band is caused by the elimination of the non-bonded lone pair N_2-2s
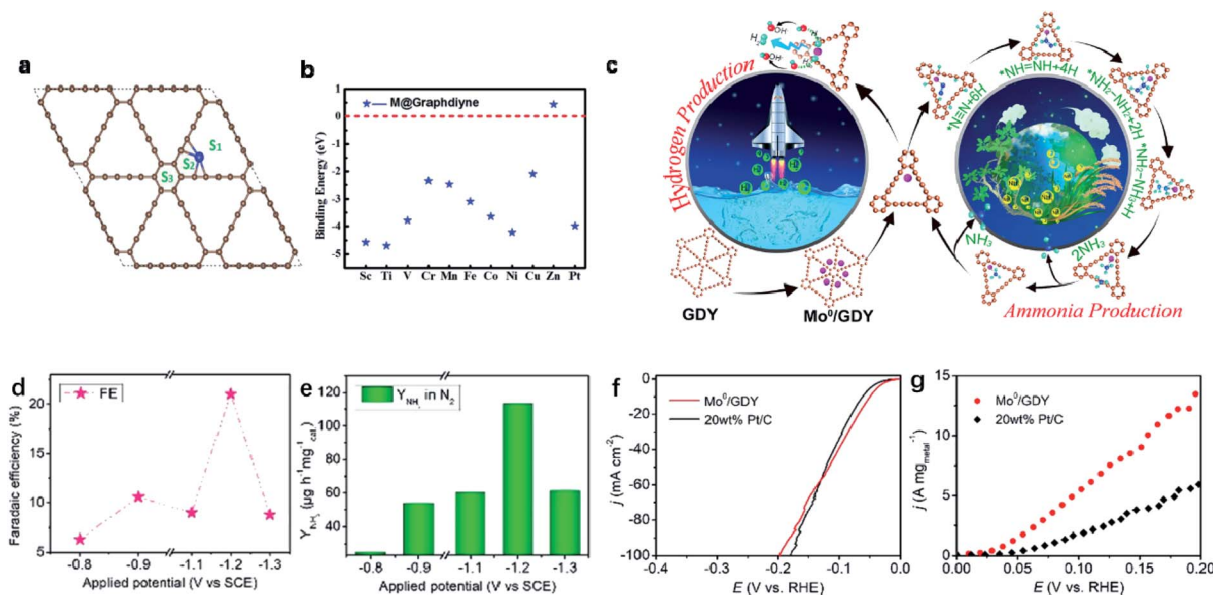

Fig. 11 (a) Different possible adsorption sites for the single TM atoms supported on GDY: (a) at the centre of the holes (S_1), at the corner of the holes (S_2) and at the centre of the hexatomic ring (S_3). (b) The corresponding binding energies for adatoms absorbing on a single GDY layer.[136] Copyright 2019 Wiley-VCH. (c) Synthesis and structural configuration evolution of the catalysis process. ECNRR performance of Mo^0/GDY. (d) FEs and (e) Y_{NH_3} at different applied potentials in 0.1 M Na_2SO_4. HER performance characteristics. (f) Polarization curves and (g) mass activities of Mo^0/GDY and 20 wt% Pt/C.[137] Copyright 2019 American Chemical Society.

This journal is © The Royal Society of Chemistry 2021

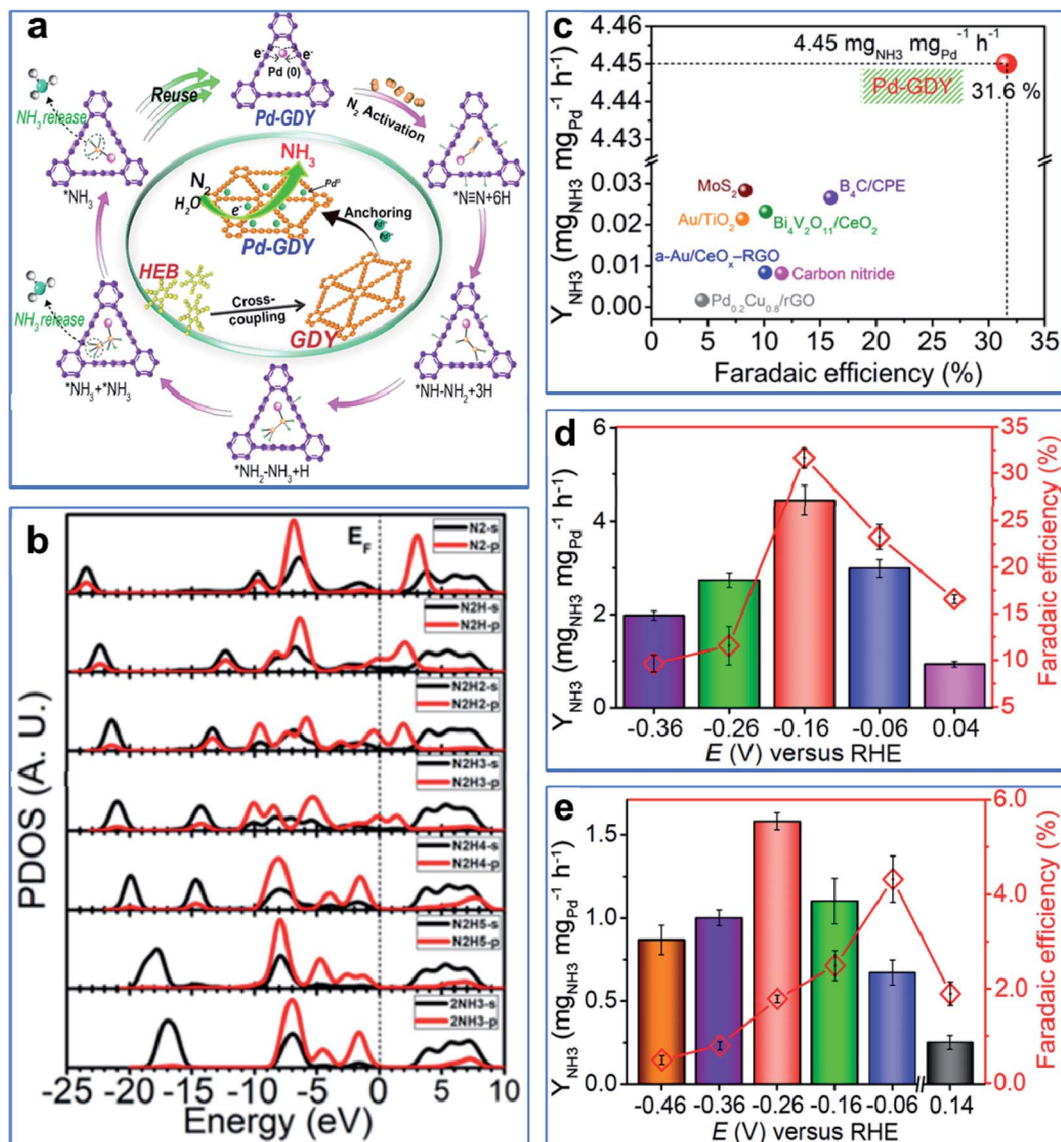*J. Mater. Chem. A*, 2021, **9**, 19298–19316 | 19311

Fig. 12 (a) Schematic of the synthesis (central green circle) and reusability of the Pd–GDY electrocatalyst for ammonia production. (b) PDOSs of s- and p-bands of all related N-species and adsorbing H among the ECNRR steps. (c) Comparison of the ECNRR performance of Pd–GDY with others. Error bars represent the calculated standard deviation from independent experiments (at least three times). (d) Y_{NH_3} and FEs at applied potentials in 0.1 M Na_2SO_4. Error bars represent the calculated standard deviation from independent experiments (at least three times). (e) Y_{NH_3} and FEs at applied potentials in 0.1 M HCl.[138] Copyright 2020 Oxford University Press.

orbital by hydrogenation of N, inhibiting the HER process. In both neutral and acidic environments, Pd–GDY exhibits excellent selectivity, activity, and stability for NRR (Fig. 12c). Under neutral conditions, this catalyst has a superhigh ammonia yield $(4.45 \pm 0.30 \ mg_{NH3} \ mg_{Pd}^{-1} \ h^{-1})$, which is nearly ten orders of magnitude higher than the ammonia yield of the currently reported nitrogen reduction catalyst, and at the same time, the FE also reached $31.62 \pm 1.06\%$. Furthermore, in an acidic environment, its catalytic activity also reaches $1.58 \pm 0.05 \ mg_{NH_3}$ $mg_{Pd}^{-1}h^{-1}$ (Fig. 12d and e). In 2021, Guo *et al.* prepared Pd/HsGDY with excellent electrochemical N_2 reduction performance, including the Faraday efficiency of 44.45% and an NH_3 yield of 115.93 mg g^{-1} h^{-1}.[139]

In order to maximize the anchoring sites in GDY, the specific surface area has to be increased by reducing the number of layers of GDY. Therefore, few-layered GDY based on 2D materials are also used to anchor heteroatoms. In 2019, Li *et al.* used graphene as a substrate to grow GDY, then anchored Pd atoms. This was used as an efficient catalyst for aromatic nitro-reduction.[140] The existence of graphene (G) acts as an epitaxy template to guarantee few-layered GDY synthesis, which enhances the specific surface area and conductivity of the GDY/G heterostructure due to its monoatomic layer and excellent electrical properties, respectively.[140]

The anchoring of metallic atoms into element-doped GDY is also possible to enhance the catalytic activity. Research on the application of transition metal and nitrogen co-doped GDY in
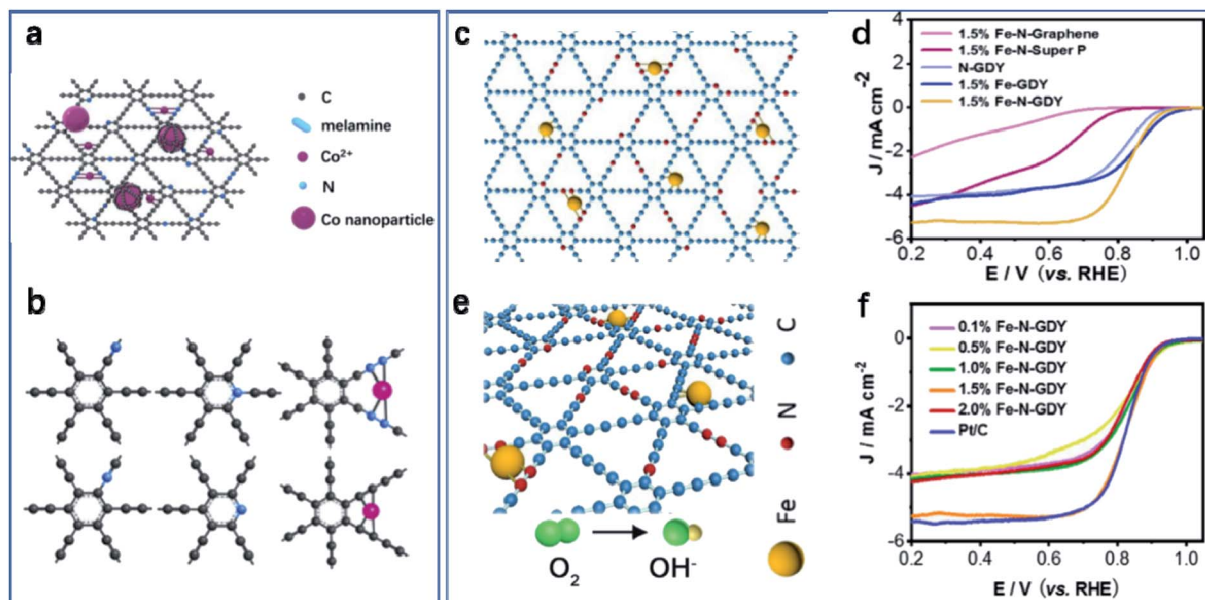
19312 | *J. Mater. Chem. A*, 2021, **9**, 19298–19316

This journal is © The Royal Society of Chemistry 2021

Fig. 13 (a) Structure of Co–N-GDY. (b) Possible catalytic sites of N and Co atoms, grey: C, blue: N, rose: Co. Copyright 2019 Carbon.[141] Copyright 2019 Published by Elsevier B.V. (c) Structure of Fe–N-GDY. (d) LSVs in O_2-saturated 0.1 M KOH at 1600 rpm. (e) Schematic diagram for the catalytic process for ORR with 1.5% Fe–N-GDY in 0.1 M KOH. (f) LSV curves of all Fe–N-GDY samples at 1600 rpm in O_2-saturated 0.1 M KOH.[142] Copyright 2019 Wiley-VCH.

catalysis has been carried out by some researchers. In 2019, Wang *et al.* prepared Co, N co-doped GDY (Co–N-GDY).[141] As shown in Fig. 13a, N atoms occupy the C position at high temperatures and become an effective active site for ORR and HER. Moreover, there is a strong interaction between Co and GDY that can improve the stability of the catalyst. Co atoms form Co–N_x and Co–C_x catalytic active sites with N and C atoms, respectively (Fig. 13b). Therefore, Co–N-GDY material is an efficient and stable dual-functional catalyst for ORR and HER. Furthermore, Si *et al.* also prepared ferrum-nitrogen co-doped GDY (Fe–N-GDY).[142] Similar to Co–N-GDY, the sites of Fe and N in a GDY network are shown in Fig. 13c. Due to the strong interaction between Fe and GDY, a relatively high Fe doping amount (Fe content is 0.1% to 2%) can be obtained by using a small amount of Fe precursors. By studying the ORR process of GDY with different Fe doping contents, it was found that the catalytic effect of Fe and N co-doping is better than that of GDY with N doping and Fe doping alone. It was also found that the best catalytic effect was achieved with 1.5% Fe doping (Fig. 13d). Due to the synergistic effect of Fe and N, 1.5% Fe–N-GDY obtained comparable catalytic activity with Pt/C in an alkaline environment and better stability (Fig. 13e and f).

Moreover, Yin *et al.* prepared a Pd single-atom catalyst (Pds-GDY) by using GDY as support in the semi-hydrogenation of alkynes in 2020.[143] In the same year, Yu *et al.* utilized GDY to anchor ruthenium atoms and exhibited high efficiency in water splitting.[144] DFT calculation indicates that GDY-supported single iron (Fe) atom (Fe/GDY) can be utilized as a catalyst for the electrocatalytic reduction of CO_2 (CO_2ER).[145] Also, GDY embedded in Ni and Cu atoms acts as an efficient catalyst for CO oxidation.[146]

4. Conclusion and prospects

GDY possesses rich acetylenic bonds, unique pore structures, which provide a huge platform for developing GDY on doping and anchoring heteroatoms. The introduction of heteroatoms into GDY is one of the important methods to change the electronic properties of GDY, providing great potential for the application of GDY in catalysis, energy storage and other fields. GDY has great prospects for applications in energy devices such as lithium-ion batteries, sodium-ion batteries, and electrocatalytic processes such as ORR, HER, and ECNRR in important industrial reactions. However, more efforts should be taken in this field, including the following:

Currently, it is still difficult to control the doping sites on carbon materials, however, the determined doping sites are of great significance for the study of the catalytic activity. At the same time, the imprecise control of doping form has a great influence on the structure of GDY, which may make it exhibit different properties. In addition, the study of precise control of the anchoring site and atom numbers of the metal element is critical to study the performance and stability of atomic catalysts. There are possible approaches to addressing these challenges including the synthesis of high-quality GDY, designation of certain chemical reactions for the introduction of heteroatoms, and control of the deposition process of metallic atoms in the triangle molecular pore of GDY. Besides, developing the large-scale fabrication approach of GDY and reducing the cost are also important. As a new carbon material, research on GDY is still in a relatively primary stage, and researchers are actively exploring the preparation method of low-cost high-quality GDY. Yin *et al.* using microwave-induced non-catalysts in solid/liquid

This journal is © The Royal Society of Chemistry 2021

J. Mater. Chem. A, 2021, **9**, 19298–19316 | **19313**

interfaces to provide a rapid and simple preparation approach for GDY.[147] Yang *et al.* utilized zinc as a substrate to obtain HsGDY with a mass of up to 0.5 g.[125] We believe that with the discovery of GDY's unique high catalytic activity, the gradual marketization of GDY will greatly reduce the cost. At the same time, we found that high catalytic activity, *i.e.*, comparable to that of noble metals, can be achieved by compositing GDY with non-noble metals, which provides a new way to reduce catalytic costs. Furthermore, the development of metal-free catalytic materials is expected to further reduce costs.

Since the fabrication of GDY in 2010, more and more scientists have invested in the research of GDY. The unique acetylene-rich and porous structure of GDY provide unlimited possibilities for precise chemical control. The introduction of heteroatoms effectively regulates local electronic structures, which makes us passionately believe that significant progress in the energy field will be achieved through continuous attempts with GDY.

Conflicts of interest

There are no conflicts to declare.

References

1 B. C. Thompson and J. M. J. Fréchet, *Angew. Chem., Int. Ed.*, 2008, **47**, 58–77.

2 R. H. Baughman, A. A. Zakhidov and W. A. De Heer, *Science*, 2002, **297**, 787–792.

3 A. K. Geim, *Science*, 2009, **324**, 1530–1534.

4 X. Gui, J. Wei, K. Wang, A. Cao, H. Zhu, Y. Jia, Q. Shu and D. Wu, *Adv. Mater.*, 2010, **22**, 617–621.

5 C. Chung, Y.-K. Kim, D. Shin, S.-R. Ryoo, B. H. Hong and D.-H. Min, *Acc. Chem. Res.*, 2013, **46**, 2211–2224.

6 P. J. F. Harris, *Int. Mater. Rev.*, 2004, **49**, 31–43.

7 J. Ge, H. Zhu, Y. Yang, Y. Xie, G. Wang, Lu. Shi, O. Schmidt and S. Yu, *CCS Chem.*, 2020, **2**, 1–12.

8 M. S. Strano, C. A. Dyke, M. L. Usrey, P. W. Barone, M. J. Allen, H. Shan, C. Kittrell, R. H. Hauge, J. M. Tour and R. E. Smalley, *Science*, 2003, **301**, 1519–1522.

9 F. Wudl, *J. Mater. Chem.*, 2002, **12**, 1959–1963.

10 S. Foley, C. Crowley, M. Smaihi, C. Bonfils, B. F. Erlanger, P. Seta and C. Larroque, *Biochem. Biophys. Res. Commun.*, 2002, **294**, 116–119.

11 C. Hu, Q. Yue, F. Zhao, Y. Zhao, B. Pan, L. Bai, X. Wang and W. Li, *CCS Chem.*, 2020, **2**, 1872–1883.

12 F. Kong, Y. Yue, Q. Li and S. Ren, *Nanomaterials*, 2021, **11**, 1161.

13 Y. Li, L. Xu, H. Liu and Y. Li, *Chem. Soc. Rev.*, 2014, **43**, 2572–2586.

14 B. Li, C. Lai, M. Zhang, G. Zeng, S. Liu, D. Huang, L. Qin, X. Liu, H. Yi, F. Xu, N. An and L. Chen, *Adv. Energy Mater.*, 2020, **10**, 2000177.

15 Z. Jin, Q. Zhou, Y. Chen, P. Mao, H. Li, H. Liu, J. Wang and Y. Li, *Adv. Mater.*, 2016, **28**, 3697–3702.

16 C. Kuang, G. Tang, T. Jiu, H. Yang, H. Liu, B. Li, W. Luo, X. Li, W. Zhang and F. Lu, *Nano Lett.*, 2015, **15**, 2756–2762.

17 H. Du, H. Yang, C. Huang, J. He, H. Liu and Y. Li, *Nano Energy*, 2016, **22**, 615–622.

18 Z. Zhang, C. Wu, Q. Pan, F. Shao, Q. Sun, S. Chen, Z. Li and Y. Zhao, *Chem. Commun.*, 2020, **56**, 3210–3213.

19 X. Kan, Y. Ban, C. Wu, Q. Pan, H. Liu, J. Song, Z. Zuo, Z. Li and Y. Zhao, *ACS Appl. Mater. Interfaces*, 2018, **10**, 53–58.

20 H. Tang, C. M. Hessel, J. Wang, N. Yang, R. Yu, H. Zhao and D. Wang, *Chem. Soc. Rev.*, 2014, **43**, 4281–4299.

21 S. Wang, L. Yi, J. E. Halpert, X. Lai, Y. Liu, H. Cao, R. Yu, D. Wang and Y. Li, *Small*, 2012, **8**, 265–271.

22 H. Shang, Z. Zuo, L. Li, F. Wang, H. Liu, Y. Li and Y. Li, *Angew. Chem., Int. Ed.*, 2018, **57**, 774–778.

23 J. Li, T. Jiu, S. Chen, L. Liu, Q. Yao, F. Bi, C. Zhao, Z. Wang, M. Zhao and G. Zhang, *Nano Lett.*, 2018, **18**, 6941–6947.

24 K. Xiao, J. Li, X. Wu, H. Liu, C. Huang and Y. Li, *Carbon*, 2019, **144**, 72–80.

25 R. Liu, H. Liu, Y. Li, Y. Yi, X. Shang, S. Zhang, X. Yu, S. Zhang, H. Cao and G. Zhang, *Nanoscale*, 2014, **6**, 11336–11343.

26 K. Wang, N. Wang, J. He, Z. Yang, X. Shen and C. Huang, *ACS Appl. Mater. Interfaces*, 2017, **9**, 40604–40613.

27 J. Li, C. Wan, C. Wang, H. Zhang and X. Chen, *Chem. Res. Chin. Univ.*, 2020, **36**, 622–630.

28 C. Lu, Y. Yang, J. Wang, R. Fu, X. Zhao, L. Zhao, Y. Ming, Y. Hu, H. Lin and X. Tao, *Nat. Commun.*, 2018, **9**, 1–11.

29 N. Yang, Y. Liu, H. Wen, Z. Tang, H. Zhao, Y. Li and D. Wang, *ACS Nano*, 2013, **7**, 1504–1512.

30 Y. Li and Y. Li, *Acta Phys.-Chim. Sin.*, 2018, **34**, 992–1013.

31 Z. Zuo and Y. Li, *Chin. J. Appl. Chem.*, 2018, **35**, 1057–1066.

32 C. Yang, H. Wang and Q. Xu, *Chem. Res. Chin. Univ.*, 2020, **36**, 10–23.

33 L. Li, Z. Zuo, F. Wang, J. Gao, A. Cao, F. He and Y. Li, *Adv. Mater.*, 2020, **32**, 2000140.

34 Y. Chen, J. Li, F. Wang, J. Guo, T. Jiu, H. Liu and Y. Li, *Nano Energy*, 2019, **64**, 103932.

35 F. Wang, Z. Zuo, L. Li, F. He and Y. Li, *Nano Energy*, 2020, **68**, 104307.

36 Z. Jin, M. Yuan, H. Li, H. Yang, Q. Zhou, H. Liu, X. Lan, M. Liu, J. Wang and E. H. Sargent, *Adv. Funct. Mater.*, 2016, **26**, 5284–5289.

37 H. Yu, Y. Xue, L. Hui, F. He, C. Zhang, Y. Liu, Y. Fang, C. Xing, Y. Li and H. Liu, *Nano Energy*, 2019, **64**, 103928.

38 G. Shi, Z. Fan, L. Du, X. Fu, C. Dong, W. Xie, D. Zhao, M. Wang and M. Yuan, *Mater. Chem. Front.*, 2019, **3**, 821–828.

39 L. Hui, Y. Xue, F. He, D. Jia and Y. Li, *Nano Energy*, 2019, **55**, 135–142.

40 C. Huang, S. Zhang, H. Liu, Y. Li, G. Cui and Y. Li, *Nano Energy*, 2015, **11**, 481–489.

41 W. Li, J. Liu, Y. Yu, G. Feng, Y. Song, Q. Liang, L. Liu, S. Lei and W. Hu, *Mater. Chem. Front.*, 2020, **4**, 1268–1273.

42 Y. Luan, F. Wang, J. Zhuang, T. Lin, Y. Wei, N. Chen, Y. Zhang, F. Wang, P. Yu, L. Mao, H. Liu and J. Wang, *EcoMat*, 2021, **3**, e12092.

43 R. Razaq, P. Li, Y. Dong, Y. Li, Y. Mao and S. Bo, *EcoMat*, 2020, **2**, e12056.

44 Z. Wei, Y. Ren, J. Sokolowski, X. Zhu and G. Wu, *InfoMat*, 2020, **2**, 483–508.

45 X. Li and J. Wang, *InfoMat*, 2020, **2**, 3–32.

46 Z.-H. Sheng, H.-L. Gao, W.-J. Bao, F.-B. Wang and X.-H. Xia, *J. Mater. Chem.*, 2012, **22**, 390–395.

47 Z. Yang, H. Nie, X. Zhou, Z. Yao, S. Huang and X. Chen, *Nano*, 2011, **6**, 205–213.

48 J. P. Paraknowitsch and A. Thomas, *Energy Environ. Sci.*, 2013, **6**, 2839–2855.

49 M. Liu, R. Zhang and W. Chen, *Chem. Rev.*, 2014, **114**, 5117–5160.

50 N. A. Kumar and J.-B. Baek, *Nanotechnology*, 2015, **26**, 492001.

51 A. Kim, M. Lee, S. Han, S. J. Kang and K. Song, *Polymer*, 2015, **39**, 956–960.

52 Z. Dai, K. Wang, L. Li and T. Zhang, *Int. J. Electrochem. Sci.*, 2013, **8**, 9384–9389.

53 R. A. Hoyt, E. M. Remillard, E. D. Cubuk, C. D. Vecitis and E. Kaxiras, *J. Phys. Chem. C*, 2017, **121**, 609–615.

54 X. Li, L. Fan, Z. Li, K. Wang, M. Zhong, J. Wei, D. Wu and H. Zhu, *Adv. Energy Mater.*, 2012, **2**, 425–429.

55 J.-Y. Liu, H.-Y. Chang, Q. D. Truong and Y.-C. Ling, *J. Mater. Chem. C*, 2013, **1**, 1713–1716.

56 B. G. Kim and H. J. Choi, *Phys. Rev. B: Condens. Matter Mater. Phys.*, 2012, **86**, 115435.

57 M. Cui, T. Hu, L. Chen, P. Li, Y. Gong, Z. Wu and S. Wang, *ChemElectroChem*, 2020, **7**, 4843–4852.

58 M. Zhang, X. Wang, H. Sun, N. Wang, Q. Lv, W. Cui, Y. Long and C. Huang, *Sci. Rep.*, 2017, **7**, 1–10.

59 Z. Feng, Y. Tang, W. Chen, D. Wei, Y. Ma and X. Dai, *Mol. Catal.*, 2020, **483**, 110705.

60 L. Bai, Z. Zheng, Z. Wang, F. He, Y. Xue and N. Wang, *Mater. Chem. Front.*, 2021, **5**, 2247–2254.

61 Z. Feng, Y. Ma, Y. Li, R. Li, Y. Tang and X. Dai, *Appl. Surf. Sci.*, 2019, **494**, 421–429.

62 Z. Feng, Y. Ma, Y. Li, R. Li, J. Liu, H. Li, Y. Tang and X. Dai, *J. Phys.: Condens. Matter*, 2019, **31**, 465201.

63 L. Hui, Y. Xue, Y. Liu and Y. Li, *Small*, 2021, 2006136.

64 Y. Guo, J. Liu, Q. Yang, L. Ma, Y. Zhao, Z. Huang, X. Li, B. Dong, X. Z. Fu and C. Zhi, *Small*, 2020, **16**, 1907341.

65 P. Autreto, J. De Sousa and D. Galvao, *Carbon*, 2014, **77**, 829–834.

66 K. Srinivasu and S. K. Ghosh, *J. Phys. Chem. C*, 2012, **116**, 5951–5956.

67 Z. Zuo and Y. Li, *Joule*, 2019, **3**, 899–903.

68 Z.-Z. Lin, *Carbon*, 2015, **86**, 301–309.

69 Z. Feng, R. Li, Y. Ma, Y. Li, D. Wei, Y. Tang and X. Dai, *Phys. Chem. Chem. Phys.*, 2019, **21**, 19651–19659.

70 X.-P. Yin, S.-F. Tang, C. Zhang, H.-J. Wang, R. Si, X.-L. Lu and T.-B. Lu, *J. Mater. Chem. A*, 2020, **8**, 20925–20930.

71 H. Shen and Q. Sun, *J. Phys. Chem. C*, 2019, **123**, 29776–29782.

72 M. Bartolomei, E. Carmona-Novillo and G. Giorgi, *Carbon*, 2015, **95**, 1076–1081.

73 Y. Xue, B. Huang, Y. Yi, Y. Guo, Z. Zuo, Y. Li, Z. Jia, H. Liu and Y. Li, *Nat. Commun.*, 2018, **9**, 1–10.

74 Y. Zhao, L. Zhang, J. Qi, Q. Jin, K. Lin and D. Wang, *Acta Phys.-Chim. Sin.*, 2018, **34**, 1048–1060.

75 J. Li, X. Gao, L. Zhu, M. N. Ghazzal, J. Zhang, C. Tung and L. Wu, *Energy Environ. Sci.*, 2020, **13**, 1326–1346.

76 Y. Zhao, H. Tang, N. Yang and D. Wang, *Adv. Sci.*, 2018, **5**, 1800959.

77 Z. Zuo, D. Wang, J. Zhang, F. Lu and Y. Li, *Adv. Mater.*, 2019, **31**, 1803762.

78 M. Zhang, Z. Guan, Z. Yang, X. Hu, X. Wang, Y. Long and C. Huang, *Chem. Mater.*, 2020, **32**, 9001–9007.

79 J. Pan, S. Du, Y. Zhang, L. Pan, Y. Zhang, H.-J. Gao and S. T. Pantelides, *Phys. Rev. B: Condens. Matter Mater. Phys.*, 2015, **92**, 205429.

80 A. Mohajeri and A. Shahsavar, *J. Mater. Sci.*, 2017, **52**, 5366–5379.

81 Y. Zheng and S.-Z. Qiao, *Nat. Chem.*, 2018, **10**, 900–902.

82 W. Zeng, Y. Zhang, X. Liu, L. Qi, W. Kang, L. Fang and M. Zhou, *Appl. Surf. Sci.*, 2020, **523**, 146468.

83 L. Arachchige, Y. Xua, Z. Dai, X. Zhang, F. Wang and C. Sun, *J. Mater. Sci. Technol.*, 2021, **77**, 244–251.

84 I. Muhammad, S. Wang, J. Liu, H. Xie and Q. Sun, *J. Renewable Sustainable Energy*, 2019, **11**, 014106.

85 Z. Feng, Y. Ma, Y. Li, R. Li, J. Liu, H. Li, Y. Tang and X. Dai, *Phys. E*, 2019, **114**, 113590.

86 X. Chen, Y. Zhang, Y. Ren, D. Wang and J. Yun, *Mater. Res. Express*, 2019, **6**, 095610.

87 K. Xu, N. Liao, M. Zhang and W. Xue, *Int. J. Hydrogen Energy*, 2020, **45**, 28893–28902.

88 H. Bu, M. Zhao, H. Zhang, X. Wang, Y. Xi and Z. Wang, *J. Phys. Chem. A*, 2012, **116**, 3934–3939.

89 J. Zhao, Z. Chen and J. Zhao, *J. Mater. Chem. A*, 2019, **7**, 4026–4035.

90 J. Gu, S. Magagula, J. Zhao and Z. Chen, *Small Methods*, 2019, **3**, 1800550.

91 Y. Jiao, A. Du, S. C. Smith, Z. Zhu and S.-Z. Qiao, *J. Mater. Chem. A*, 2015, **3**, 6767–6771.

92 B. K. Das, D. Sen and K. Chattopadhyay, *Phys. Chem. Chem. Phys.*, 2016, **18**, 2949–2958.

93 T. He, L. Zhang, G. Kour and A. Du, *J. CO2 Util.*, 2020, **37**, 272–277.

94 J. Li, X. Gao, L. Zhu, M. N. Ghazzal, J. Zhang, C.-H. Tung and L.-Z. Wu, *Energy Environ. Sci.*, 2020, **13**, 1326–1346.

95 L. Dai, Y. Xue, L. Qu, H.-J. Choi and J.-B. Baek, *Chem. Rev.*, 2015, **115**, 4823–4892.

96 M. Shao, Q. Chang, J.-P. Dodelet and R. Chenitz, *Chem. Rev.*, 2016, **116**, 3594–3657.

97 S. K. Bikkarolla, P. Cumpson, P. Joseph and P. Papakonstantinou, *Faraday Discuss.*, 2014, **173**, 415–428.

98 E. P. Randviir and C. E. Banks, *Electroanalysis*, 2014, **26**, 76–83.

99 D. Guo, R. Shibuya, C. Akiba, S. Saji, T. Kondo and J. Nakamura, *Science*, 2016, **351**, 361–365.

100 Y. Nie, L. Li and Z. Wei, *Chem. Soc. Rev.*, 2015, **44**, 2168–2201.

101 F. Jaouen, E. Proietti, M. Lefèvre, R. Chenitz, J.-P. Dodelet, G. Wu, H. T. Chung, C. M. Johnston and P. Zelenay, *Energy Environ. Sci.*, 2011, **4**, 114–130.

This journal is © The Royal Society of Chemistry 2021

J. Mater. Chem. A, 2021, **9**, 19298–19316 | **19315**

102 L. Yang, S. Jiang, Y. Zhao, L. Zhu, S. Chen, X. Wang, Q. Wu, J. Ma, Y. Ma and Z. Hu, *Angew. Chem., Int. Ed.*, 2011, **50**, 7132–7135.

103 S. Guo, S. Zhang and S. Sun, *Angew. Chem., Int. Ed.*, 2013, **52**, 8526–8544.

104 Q. Lv, W. Si, Z. Yang, N. Wang, Z. Tu, Y. Yi, C. Huang, L. Jiang, M. Zhang and J. He, *ACS Appl. Mater. Interfaces*, 2017, **9**, 29744–29752.

105 Y. Zhao, J. Wan, H. Yao, L. Zhang, K. Lin, L. Wang, N. Yang, D. Liu, L. Song and J. Zhu, *Nat. Chem.*, 2018, **10**, 924–931.

106 T. Lu, X. Hu, J. He, R. Li, J. Gao, Q. Lv, Z. Yang, S. Cui and C. Huang, *Nano Energy*, 2021, **85**, 106024.

107 S. Zhang, H. Du, J. He, C. Huang, H. Liu, G. Cui and Y. Li, *ACS Appl. Mater. Interfaces*, 2016, **8**, 8467–8473.

108 T. Jiang, K. Chen, J. Wang, Z. Hu, G. Wang, X.-D. Chen, P. Sun, Q. Zhang, C. Yan and L. Zhang, *J. Mater. Chem. A*, 2019, **7**, 27535–27546.

109 X. Shen, Z. Yang, K. Wang, N. Wang, J. He, H. Du and C. Huang, *ChemElectroChem*, 2018, **5**, 1435–1443.

110 X. Liu, Y. Jiao, Y. Zheng, M. Jaroniec and S.-Z. Qiao, *J. Am. Chem. Soc.*, 2019, **141**, 9664–9672.

111 S. Zhao, S. Lu, L. Wang, J. Gale and R. Amal, *Adv. Mater.*, 2019, **31**, 1805367.

112 H. Zou, W. Rong, B. Long, Y. Ji and L. Duan, *ACS Catal.*, 2019, **9**, 10649–10655.

113 M. Zhang, H. Sun, X. Wang, H. Du, J. He, Y. Long, Y. Zhang and C. Huang, *J. Phys. Chem. C*, 2019, **123**, 5010–5016.

114 Z. Yang, W. Cui, K. Wang, Y. Song, F. Zhao, N. Wang, Y. Long, H. Wang and C. Huang, *Chem.–Eur. J.*, 2019, **25**, 5643–5647.

115 M. Salavati, N. Alajlan and T. Rabczuk, *Appl. Sci.*, 2021, **11**, 2308.

116 X. Shen, X. Li, F. Zhao, N. Wang, C. Xie, J. He, W. Si, Y. Yi, Z. Yang and X. Li, *2D Mater.*, 2019, **6**, 035020.

117 Z. Zhao and Z. Xia, *ACS Catal.*, 2016, **6**, 1553–1558.

118 Y. Zhao, N. Yang, H. Yao, D. Liu, L. Song, J. Zhu, S. Li, L. Gu, K. Lin and D. Wang, *J. Am. Chem. Soc.*, 2019, **141**, 7240–7244.

119 H. Zhang, M. Zhao, X. He, Z. Wang, X. Zhang and X. Liu, *J. Phys. Chem. C*, 2011, **115**, 8845–8850.

120 N. Wang, J. He, Z. Tu, Z. Yang, F. Zhao, X. Li, C. Huang, K. Wang, T. Jiu and Y. Yi, *Angew. Chem., Int. Ed.*, 2017, **56**, 10740–10745.

121 X. Shen, J. He, K. Wang, X. Li, X. Wang, Z. Yang, N. Wang, Y. Zhang and C. Huang, *ChemElectroChem*, 2019, **12**, 1342–1348.

122 H. Kang, Y. Chen, L. Xu, Y. Lin, Q. Feng, H. Yao and Y. Zheng, *RSC Adv.*, 2019, **9**, 31406–31412.

123 J. He, T. Lu, K. Wang, X. Wang, X. Li, X. Shen, J. Gao, W. Si, Z. Yang and C. Huang, *Adv. Funct. Mater.*, 2021, **31**, 2005933.

124 Q. Yang, Y. Guo, B. Yan, C. Wang, Z. Liu, Z. Huang, Y. Wang, Y. Li, H. Li and L. Song, *Adv. Mater.*, 2020, **32**, 2001755.

125 Q. Yang, Y. Guo, J. Gu, N. Li, C. Wang, Z. Liu, X. Li, Z. Huang, S. Wei, S. Xu, L. Song, J. Fan, Z. Chen, J. Qiu and C. Zhi, *Nano Energy*, 2020, **78**, 105283.

126 J. He, N. Wang, Z. Cui, H. Du, L. Fu, C. Huang, Z. Yang, X. Shen, Y. Yi and Z. Tu, *Nat. Commun.*, 2017, **8**, 1–11.

127 S. Kong, D. Cai, G. Li, X. Xu, S. Zhou, X. Ding, Y. Zhang, S. Yang, X. Zhou and H. Nie, *Nanoscale*, 2021, **13**, 3817–3826.

128 X. Ren, X. Li, Z. Yang, X. Wang, J. He, K. Wang, J. Yin, J. Li and C. Huang, *ACS Sustainable Chem. Eng.*, 2020, **8**, 2614–2621.

129 Z. Yang, X. Shen, N. Wang, J. He, X. Li, X. Wang, Z. Hou, K. Wang, J. Gao, T. Jiu and C. Huang, *ACS Appl. Mater. Interfaces*, 2018, **11**, 2608–2617.

130 T. Lu, J. He, R. Li, K. Wang, Z. Yang, X. Shen, Y. Li, J. Xiao and C. Huang, *Energy Storage Materials*, 2020, **29**, 131–139.

131 J. Gao, N. Wang, J. He, Z. Yang and C. Huang, *2D Materials*, 2020, **7**, 025032.

132 H. Shang, Z. Zuo, H. Zheng, K. Li, Z. Tu, Y. Yi, H. Liu, Y. Li and Y. Li, *Nano Energy*, 2018, **44**, 144–154.

133 F. Wang, Z. Zuo, L. Li, K. Li, F. He, Z. Jiang and Y. Li, *Angew. Chem., Int. Ed.*, 2019, **58**, 15010–15015.

134 B. Qiao, A. Wang, X. Yang, L. F. Allard, Z. Jiang, Y. Cui, J. Liu, J. Li and T. Zhang, *Nat. Chem.*, 2011, **3**, 634–641.

135 X.-F. Yang, A. Wang, B. Qiao, J. Li, J. Liu and T. Zhang, *Acc. Chem. Res.*, 2013, **46**, 1740–1748.

136 T. He, S. K. Matta, G. Will and A. Du, *Small Methods*, 2019, **3**, 1800419.

137 L. Hui, Y. Xue, H. Yu, Y. Liu, Y. Fang, C. Xing, B. Huang and Y. Li, *J. Am. Chem. Soc.*, 2019, **141**, 10677–10683.

138 H. Yu, Y. Xue, L. Hui, C. Zhang, Y. Fang, Y. Liu, X. Chen, D. Zhang, B. Huang and Y. Li, *Natl. Sci. Rev.*, 2020, DOI: 10.1039/nsr/nwaa213.

139 Y. Guo, J. Liu, Q. Yang, P. Khemthong, Z. Huang, Y. Zhao, Z. Chen, B. Dong, X. Fu, J. Luo and C. Zhi, *Nano Energy*, 2021, **86**, 106099.

140 J. Li, L. Zhong, L. Tong, Y. Yu, Q. Liu, S. Zhang, C. Yin, L. Qiao, S. Li and R. Si, *Adv. Funct. Mater.*, 2019, **29**, 1905423.

141 X. Wang, Z. Yang, W. Si, X. Shen, X. Li, R. Li, Q. Lv, N. Wang and C. Huang, *Carbon*, 2019, **147**, 9–18.

142 W. Si, Z. Yang, X. Wang, Q. Lv, F. Zhao, X. Li, J. He, Y. Long, J. Gao and C. Huang, *ChemSusChem*, 2019, **12**, 173–178.

143 X. Yin, S. Tang, C. Zhang, H. Wang, R. Si, X. Lu and T. Lu, *J. Mater. Chem. A*, 2020, **8**, 20925–20930.

144 H. Yu, L. Hui, Y. Xue, Y. Liu, Y. Fang, C. Xing, C. Zhang, D. Zhang, X. Chen and Y. Du, *Nano Energy*, 2020, **72**, 104667.

145 X. Liu, Z. Wang, Y. Tian and J. Zhao, *J. Phys. Chem. C*, 2020, **124**, 3722–3730.

146 X. Liu, W. Tang, S. Liu, X. Chen, Y. Li, X. Hu, L. Qiao and Y. Zeng, *Appl. Surf. Sci.*, 2021, **539**, 148287.

147 C. Yin, J. Li, T. Li, Y. Yu, Y. Kong, P. Gao, H. Peng, L. Tong and J. Zhang, *Adv. Funct. Mater.*, 2020, **30**, 2001396.

19316 | *J. Mater. Chem. A*, 2021, **9**, 19298–19316

This journal is © The Royal Society of Chemistry 2021